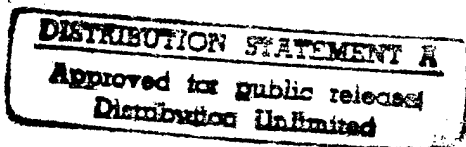



ADVANCED SCIENCE & TECHNOLOGY CENTRE

Contract No. 00014-93-C-0217

DESIGN STUDY OF ARCTIC CAPABLE
LOW FREQUENCY ACOUSTIC SOURCE

TECHNICAL REPORT




Mark Slavinsky
Principal Investigator

19971030 077

Nizhny Novgorod, Russia, 1993

DTIC QUALITY INSPECTED 6

The work has been fulfilled by:

Alelekov I.V.
Artel'nyi V.V.
Barashkov A.D.
Bogolubov B.N.
Dubovoi Yu.A.
Erkin A.F.
Goldovsky B.I.
Kabin V.S.
Kapustin P.A.
Klimov V.A.
Kolodieva I.I.
Korotin P.I.
Krapivin V.P.
Modina I.V.
Pigalov K.E.
Rybenkov L.A.
Siz'min A.M.
Slavinsky M.M.
Smirnov S.Yu.
Zharov A.I.

Translated by Rudic, N.V.

TABLE OF CONTENTS

1.	INTRODUCTION	2
2.	EMITTER PROTOTYPE	5
2.1.	Calculation of prototype parameters	9
2.2.	Numerical simulation of oscilating system of prototype	13
2.3.	Results of prototype tests	19
3.	CALCULATION OF PARAMETERS AND NUMERICAL SIMULATION OF THE ARCTIC SOURCE OSCILATING SYSTEM	32
4.	CONCLUSION	49
	REFERENCES	50

1. INTRODUCTION

The report deals with design conception of a low-frequency emitter with a resonant frequency 20 Hz for use during the Arctic Feasibility Acoustic Propagation Pilot Test (AFAPPT), with the results of numerical simulating an oscillation system, the calculation of basic parameters of the emitter and its prototype, of acoustic and vibromechanic tests of the prototype, and with the state-of-the-art of arranging the production and fabrication of the Arctic Source.

The suggested design of the Arctic Source is the result of more than ten-year experience of the development and operation of efficient low-frequency emitters in exploration of remote acoustic methods of the ocean diagnostics. During this period there were developed theoretical models of monopole emitters with spaced elastic elements used as the main oscillating or radiating surfaces. A large number of materials (different grade steels, titanium and aluminium - bearing alloys of different qualities) have been investigated under various conditions of hot working and machining, the resistance of these materials to alternating dynamic loads have been determined experimentally. The fatigue curves have been recorded enabling one to predict the permissible number of the emitter operating cycles in sea water.

The theory and appropriate computer programs have been developed which are capable of optimizing the profiles of the spaced elastic elements and, thus, to reduce the stress in the material to allowed limits and to simultaneously increase the equivalent emitting area and the emission frequency range.

Theoretical models have been formulated on this basis and single-mode spaced oscillating systems have been developed to provide efficient conversion of the electric energy into the acoustic one in the operating frequency range and practically complete suppression of parasitic (higher-frequency) oscillation shapes of the emitter.

The performed investigations and specially designed technologies were used when creating a family of emitters in the

frequency range of 100-600 Hz. The emitters with central frequencies of about 130 Hz and 230 Hz were manufactured in small batches and demonstrated high reliability during a number of years. Broad functional capabilities of these emitting systems have been proved in joint tests carried out by the Russian-American group of experts at the Naval Underwater Systems at the Lake Seneca during July 1992 [1,2].

New researches which promoted the advance into the frequency range under 100 Hz were used when designing the emitters with the resonance frequencies 65 Hz and 20 Hz. The same design and technologies were employed in both emitters. An emitter with the resonant frequency 65 Hz is, actually, an operating prototype of the Arctic Source.

Numerical simulation of the oscillating system has been performed and the basic parameters of the prototype have been calculated including profiles of oscillations and stresses in elastic elements and radiating pistons, the frequency spectrum and natural oscillations shapes of the emitter. A special measuring test bench was used to perform vibromechanic tests of the prototype, to investigate the frequency spectrum and the main shapes of the forced oscillations under broad-band and narrow-band excitation including those produced by the issued emitter excitation electron system. Acoustic tests of the prototype has been performed, the amplitude-frequency and phase-frequency dependences as well as the dependences of the efficiency on the acoustic power frequency and of the emission level on the excitation current have been studied [3]. The simulation results are in good agreement with experimental data. This permits to predict with high reliability the characteristics of the Acoustic Source with the resonant frequency 20 Hz using the method approved in the prototype.

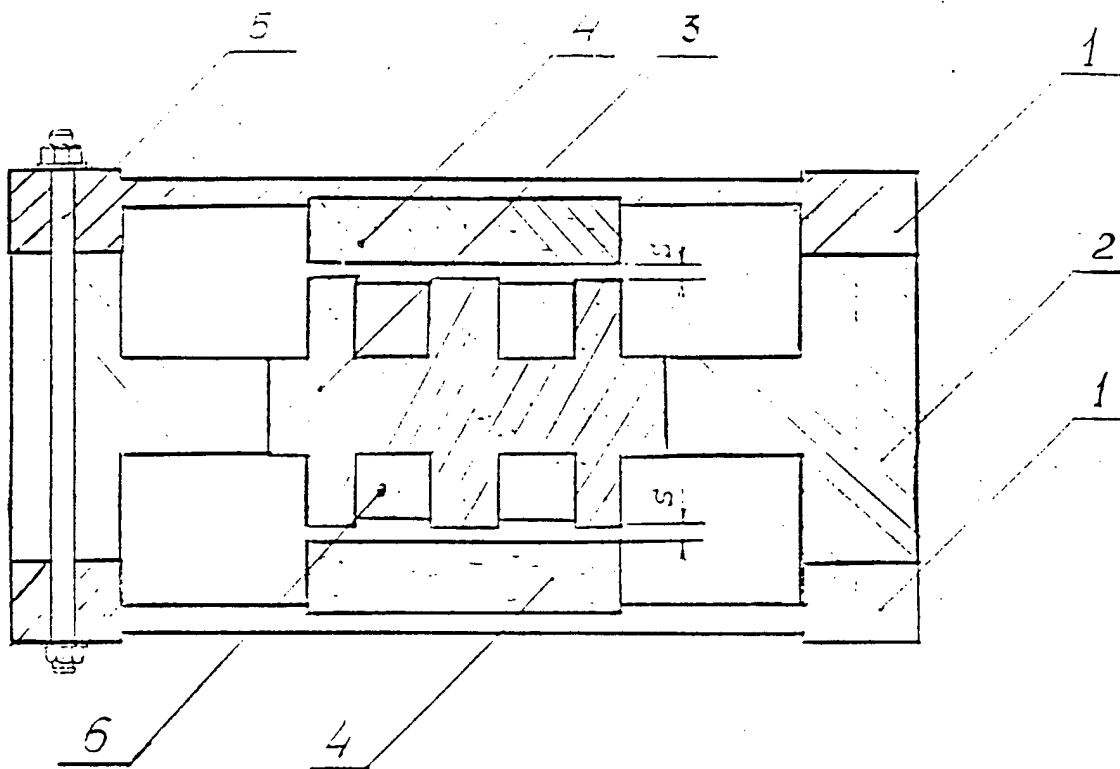
This method was employed for calculating the parameters and numerical simulating the Arctic Source design and parameters, including profiles and stresses in elastic elements and emitting pistons, the frequency spectra and main shapes of natural oscillations. Sketches of the main design elements and of the emitter assembly have been drawn. The plant responsible for the emitter fabrication has been found, the emitter design and technological background of the production have been analysed,

problems of supply with materials and components have been considered, the schedule of the emitter fabrication have been prepared.

2. Emitter prototype

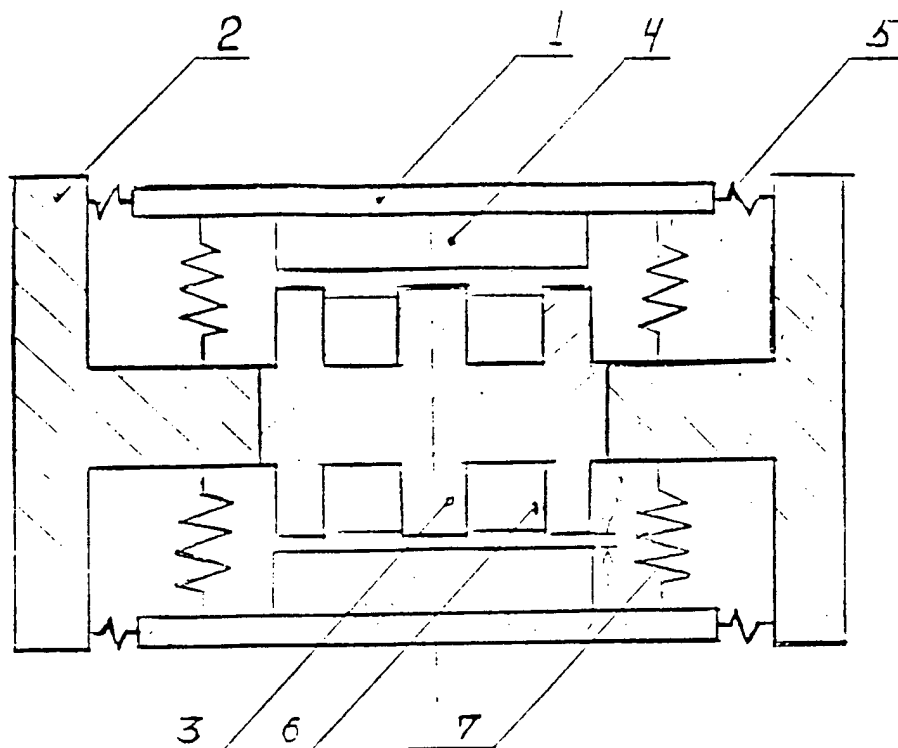
In the conventional electromagnetic emitter design (fig.2.1) two elastic plates (membranes) 1 are used as an emitting surface, the centre of which is connected to the moving parts 4 of the electromagnet core. The fixed part 3 of the electromagnet core with the field coil 6 is housed in the case 2, to which both membranes are rigidly fixed by the bolts 5. The resonance frequency of the emitter is determined, on the one hand, by the associated mass of water and the equivalent oscillating mass of a membrane and, on the other hand, by the elasticity of the membranes dependent on their material and geometry.

When developing emitters at the frequencies lower than 100 Hz, of special importance is the design with maximum emitting area. There are principal limitations from this point of view in conventional membrane emitters. It is impossible to provide larger emitting area of a membrane than half of its total area. The maximum emitting area is ensured in a oscillating piston (fig.2.2). The idea of the piston electromagnetic emitter has long been known. The main difficulty encountered in designing such an emitter is the creation of a mechanical vibrating system in which the reciprocating motion of the pistons 1 is stable and other types of oscillations have much higher eigenfrequencies than the operating one and, thus, are not excited while the emitter is operating. In this emitter, as distinct from the membrane one, large emitting area and the elasticity governing the resonance frequency cannot be combined in one unit. An additional element is introduced, that is the spring 7. Besides there arises the problem of providing hermetic decoupler 5 of the vibrating piston and the case 2. The decoupling should be rigid enough to prevent acoustic locking of the emitter, to bear multicyclic variable load and essential excess static pressure occurred at descent and ascent, and to minimize mechanical losses in order to provide high efficiency of the emitter. The calculation for the piston electromagnetic emitter will be given below, in the design of which all these difficulties have been resolved and the membrane emitter idea has been conserved by employing thoroughly elaborated



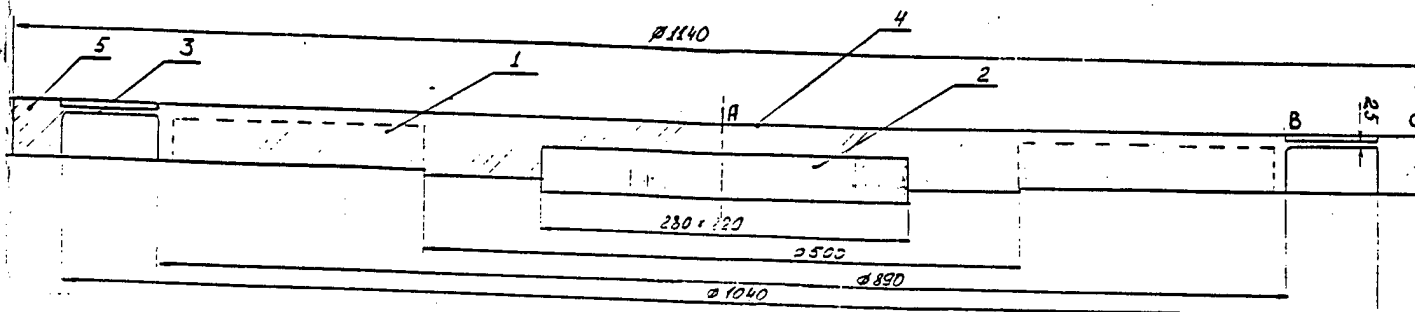
- 1 - Membrane
- 2 - Case
- 3 - Electromagnet Core (fixed part)
- 4 - Electromagnet Core (moving part)
- 5 - Bolts
- 6 - Field Coil
- S - Gap between field poles

2.1 Hydroacoustic source of membrane type.
Schematic assembly drawing.



- 1 - Piston
- 2 - Case
- 3 - Electromagnet Core (fixed part)
- 4 - Electromagnet Core (moving part)
- 5 - Hermetic decoupler
- 6 - Field Coil
- 7 - Spring
- S - Gap between field poles

2.2 Hydroacoustic source of piston type.
Schematic assembly drawing.



- 1 - Piston part
- 2 - Electromagnet Core (moving part)
- 3 - Hermetic decoupler
- 4 - Radiating surface
- 5 - Flange

optimization methods and technological techniques.

2.1. Calculation of prototype parameters

The emitter has two identical radiating elements shown in fig.2.3. A radiating element is made of a single metal piece and has the radiating piston 1, the elastic decoupler 3, the moving part of the electromagnet core 2 and the flange 5. The piston is designed as a rebbed honeycomb sandwich structure, so that to reduce its mass and conserve the necessary rigidity. The eigenfrequencies of the piston oscillating in water should be much larger than the operating frequency. The associated mass of water for one piston is close to that of the piston oscillating in an infinitely rigid screen and can be calculated by the equation:

$$M_a = \frac{8}{3} \rho R^3, \quad (1)$$

where R is the effective radius of the piston and decoupler and ρ is the water density. In the prototype $R = 0.485$ m and $M_a = 304$ kg. The design calculation has yielded that the oscillating mass of the piston is 65 kg, while the mass of the moving part of the electromagnetic core attached to it is $M_m = 16$ kg. Therefore, the total oscillating mass $M_k = 81$ kg is 3.7 times smaller than the associated mass of water and, hence, the frequency band of this emitter is close to the maximum possible one. Note that in this mass ratio, the resonance frequency of the piston oscillating in air is twice as large as its resonance frequency in water. The emitting area of this emitter is $S_1 = 1.478$ m² and, thus, the radius of the equivalent sphere amounts to $R_1 = 0.34$ m. The expected relative frequency band of the mechanical oscillating system is yielded by

$$\delta f = \frac{2\pi f R_1}{v_{ma} C} \times \frac{M_a}{M_a + M_k}, \quad (2)$$

when C is the sound velocity in water, f is the resonance frequency of the emitter, and v_{ma} is the mechanoacoustic efficiency of the emitter. In the prototype $\delta f = 8\%f$. In order to obtain the required relative frequency band 25%, the magnetic system is to

have the reserve of strength of 2.25 times.

The elastic decoupler 3 bears alternating loads when the emitter is oscillating and static loads caused by the static pressure of air and water when the emitter is descending or ascending. Let us consider these loads separately. The radiation level 201 dB is achieved in the prototype at the piston vibration amplitude equal to 1 mm. Figure 2.4 illustrates the mechanical stress distribution and the oscillation profile of the piston with the decoupler when the emitter is operating in water. The in-phase oscillations of the decoupler and the piston prove the absence of acoustic locking. The maximum mechanical stress in the decoupler is 7.5 kg/sq.mm. If the piston stroke limiters are provided, the emitter is capable of withstanding the excess static air pressure of 3 technical atmospheres and promotes descent and ascent.

The resonance frequency of the emitter is determined by the membrane elasticity of the spring with optimized geometry. Figure 2.5 exhibits the mechanical stress distribution in the membrane at the nominal radiated power. The maximum stress occurred at the edges of operating sections of the membrane are low and do not exceed 6.2 kg/sq.mm.

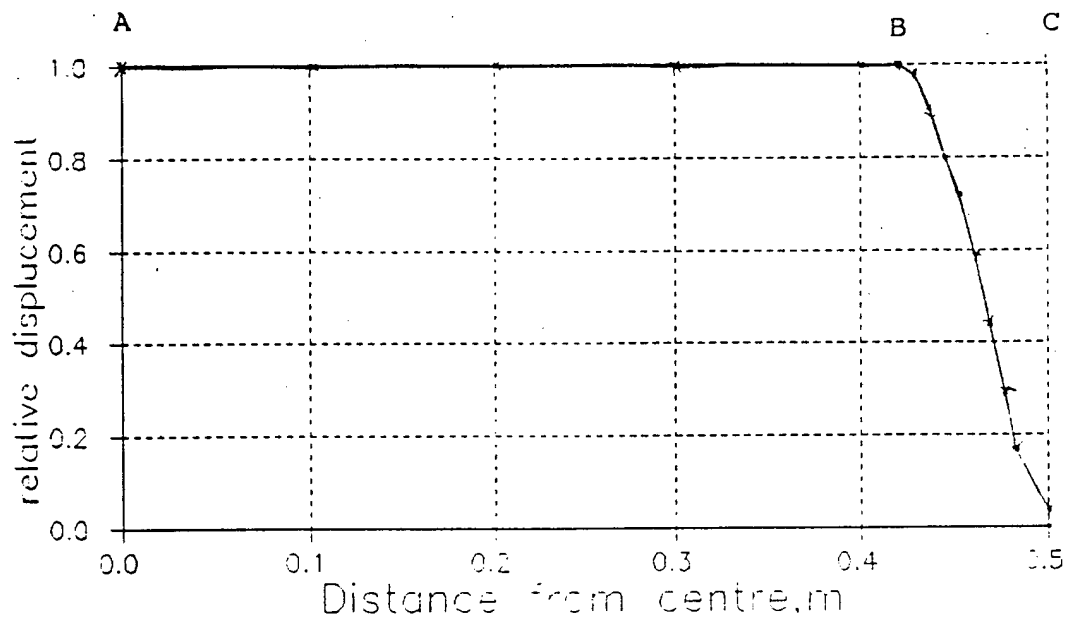
The limiting acoustic power of the emitter at the resonance frequency depends on the magnetic system capabilities and is given by

$$N = v_{ma} \frac{\pi C B^4}{2 \mu_o^2 \rho \omega^2} \times \frac{S_m^2}{S_1^2}, \quad (3)$$

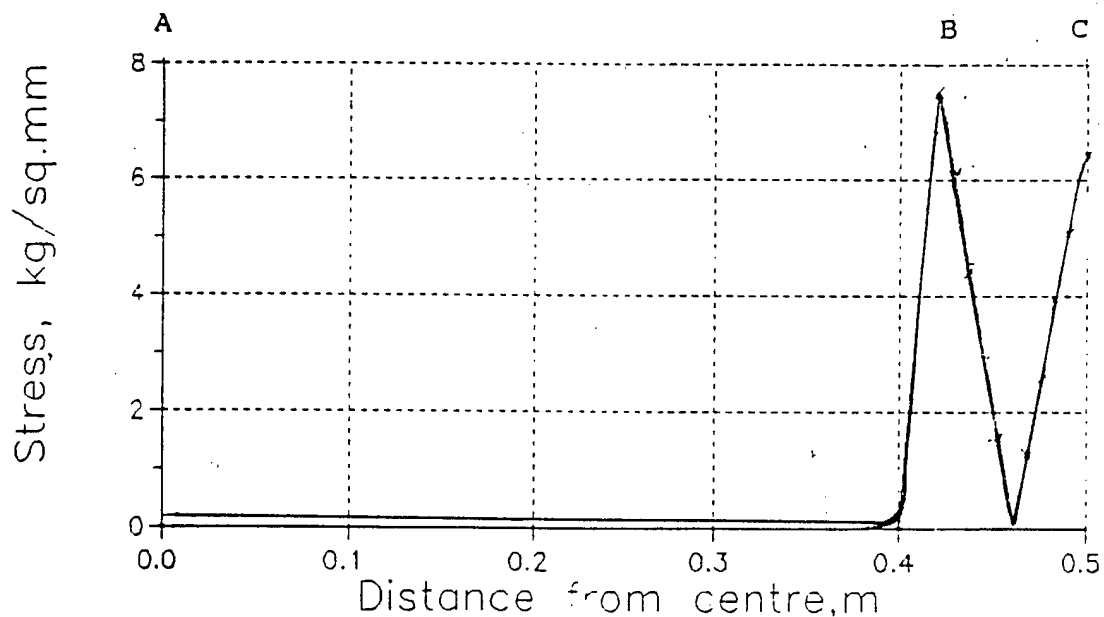
where B is the admissible induction in the electromagnet core material, ω is the circular frequency, S_m is the cross-section of the electromagnet core and S_{p1} is the emitting area of the piston. For the prototype $S_m = 0.021$ sq.m, $S_1 = 0.739$ sq.m, $v_{ma} = 0.8$ we obtain $N = 45$ kW. Since the nominal power is 1kW, the reserve of strength in this structure is 6.7 times, which is much larger than the required one equal to 2.25 times. Therefore, the magnetic system of the emitter is capable of 4 kW sound emitting in the relative band of 25%.

The core cross-section and the number of loops in the field coil are chosen so that to ensure the electromechanic efficiency

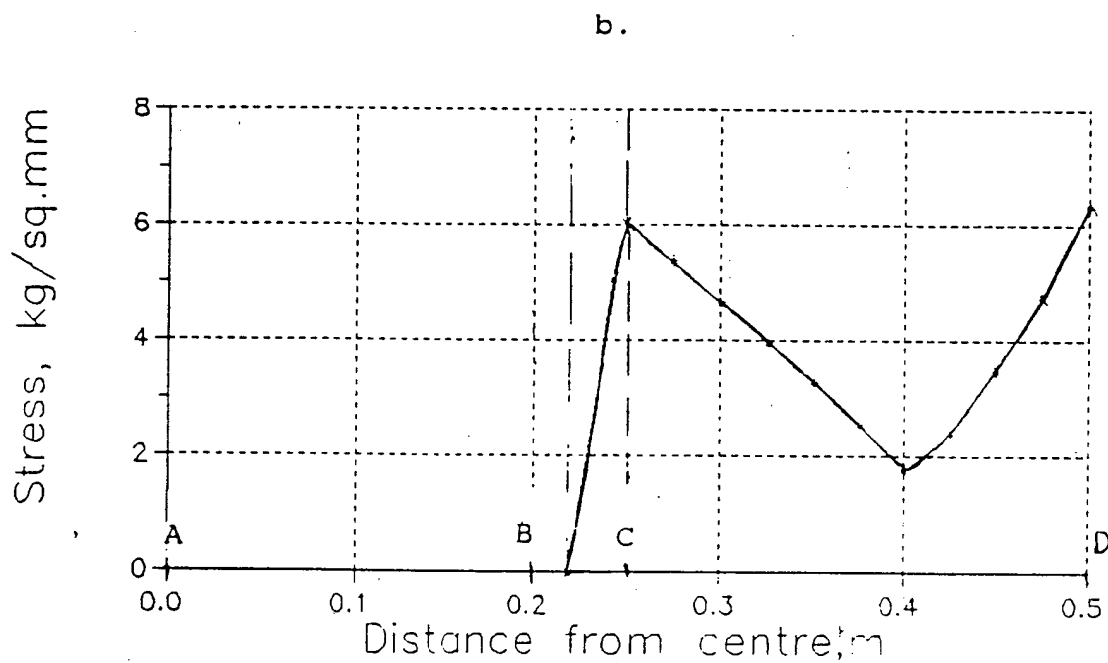
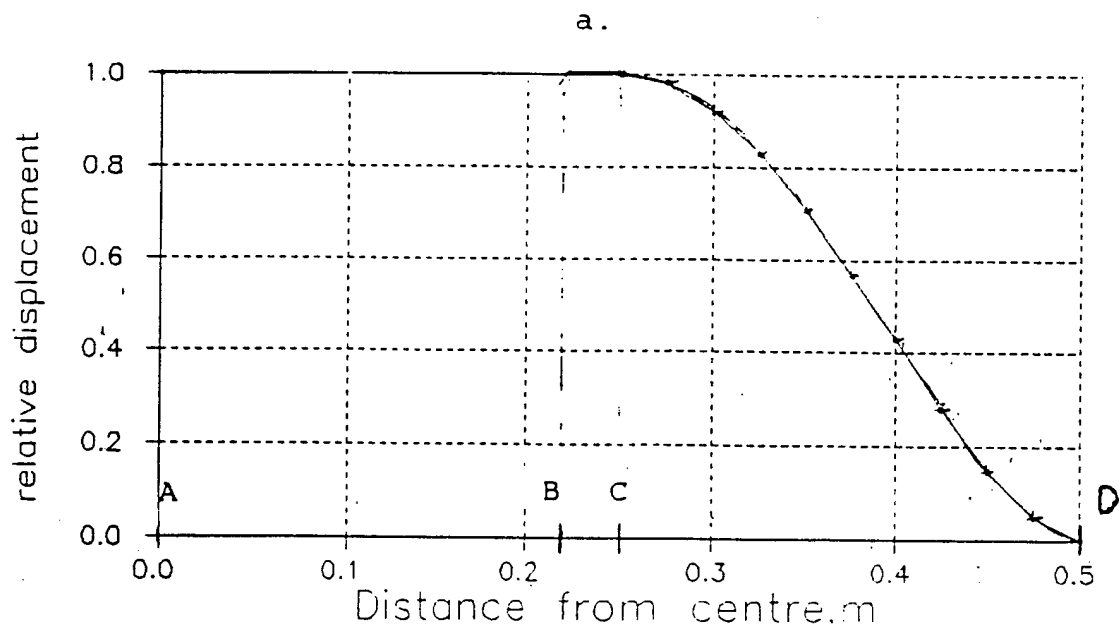
a.



b.



2.4 Prototype. Radiating element. Calculation.
Relative displacement (a) and stress (b) profiles
(Displacement amplitude 1 mm).
Section AB - piston part, section BC - decoupler.



2.5 Prototype. Membrane (spring). Calculation.
 Relative displacement (a) and stress (b) profiles
 (Displacement amplitude 1 mm).
 Section AB - inside flange, section BC - spring
 element.

of the emitter 70% , the average current and the coil voltage (for 1kW of the radiated power at the resonance frequency) 20A and 500V, respectively, at the frequency band edges 30A and 1500V.

The performed calculations of the mechanical loads have shown that the D16T aluminium alloy used for the prototype fabrication provides the service life of more than $2 \cdot 10^8$ cycles. This follows from the consideration of the experimental fatigue curves for various metals and alloys (fig. 2.6). The prototype on the scale of 1:5 is shown in fig. 2.7 and its calculated parameters are presented below.

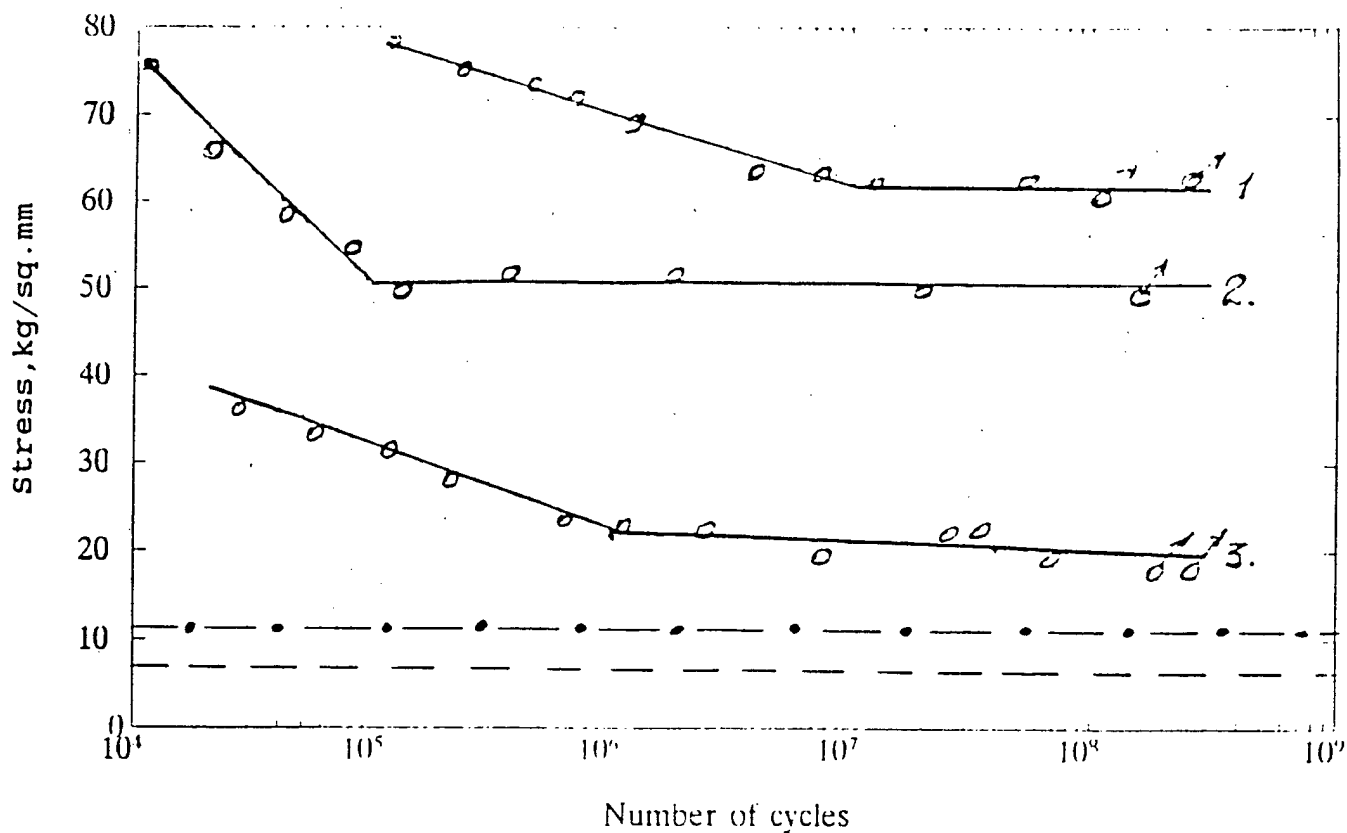
2.2. Numerical simulation of oscillating system of prototype.

The objective of the numerical simulation is to determine the frequency and shape of the fundamental mode of the prototype in air as well as the frequencies and shapes of the modes having the frequencies close to that of the fundamental one.

The numerical simulation was performed by the finite element method in the small deformation approximation using the ANSYS program set. The preliminary finite-element model of the prototype included 663 units and 412 axially symmetric elements.

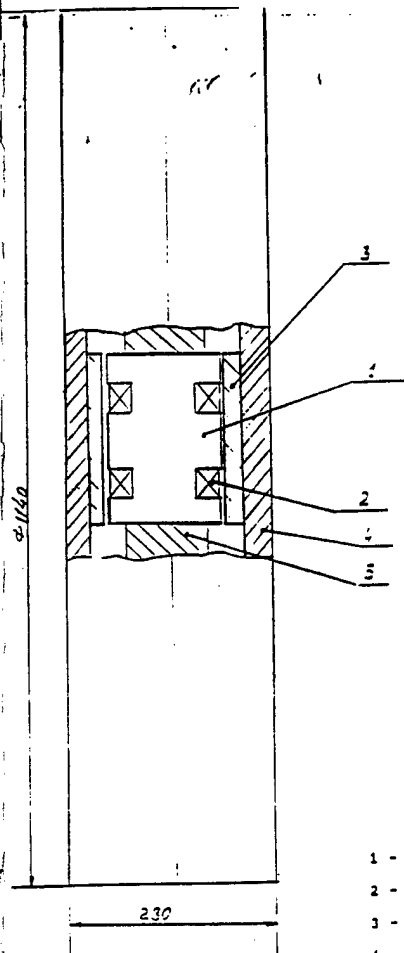
In the case of the axially symmetric structure vibrations, the dependence of displacements, deformations and stresses on the azimuth angle ϕ has the form $\cos(n\phi)$, where n is the azimuth angle taken in the plane normal to the axis of axial symmetry of the structure.

Figure 2.8 depicts the location of the first 23 modes with the azimuth indices $n = 0, 1$ and 2 on the frequency axis. The number, frequency, azimuth angle and the mode shape of the structure for each mode are given in Table 1.1. The operating mode of the prototype is mode No.1. Its frequency in air is 165 Hz. The shape of the first mode shown in fig. 2.9a is of the monopole character and represents antiphase displacements of pistons in a fixed case. Mode No.2 has the frequency 182 Hz and its shape is an in-phase displacement of pistons. The larger the mass of the case (with the electromagnet) of the emitter, the closer the second mode frequency in air to the frequency of the first mode. Note, however, that the difference between the frequencies of the first



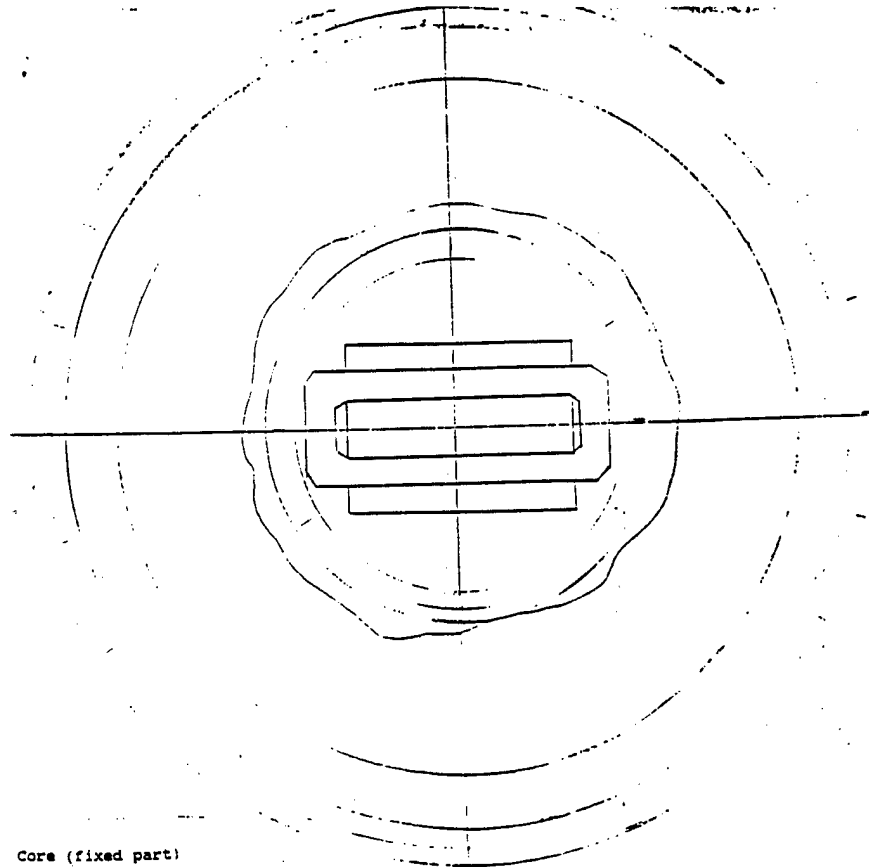
2.6 Experimental curves of fatigue for metal samples under cyclic loads: 1 - steel (type VKS - 210), 2 - titanium (type 5V), 3 - duraluminium (type D16T).

- - - - - shows stress in prototype and 20 Hz source at nominal radiation level
- shows stress in prototype and 20 Hz source at maximal radiation level

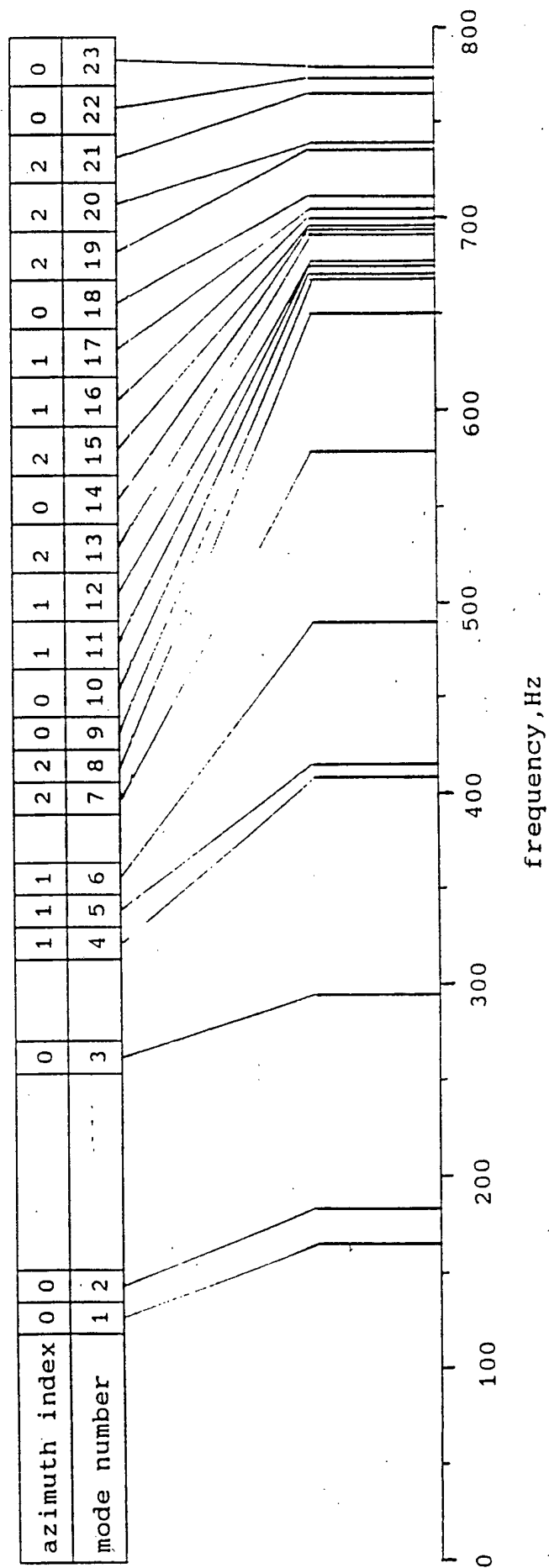


- 1 - Electromagnet Core (fixed part)
- 2 - Field Coil
- 3 - Electromagnet Core (moving part)
- 4 - Piston
- 5 - Case

15



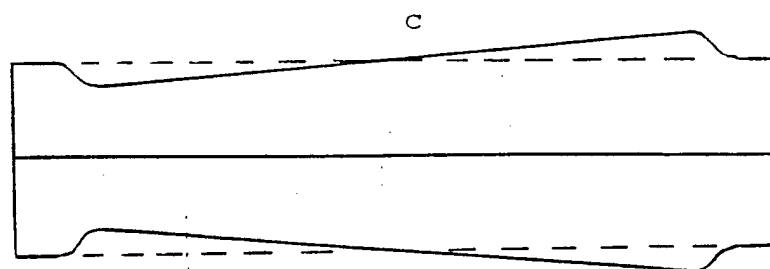
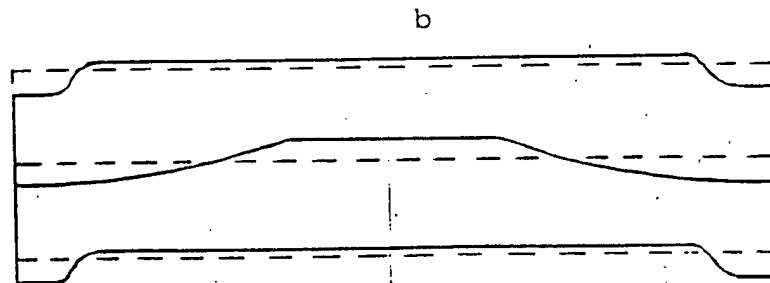
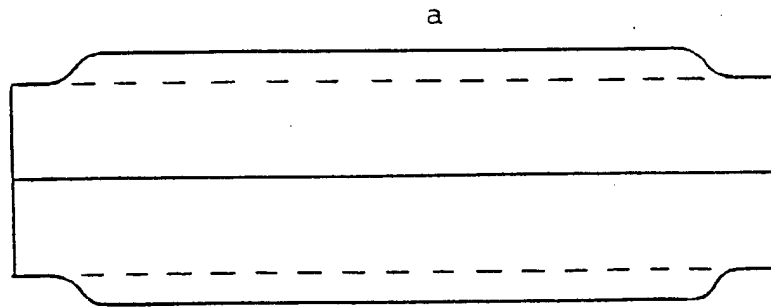
2.7 Prototype.
Scale 1:5



2.8 Prototype. Calculation (in air).
Mode frequencies.

Mode number	Frequency Hz	Azimuth index	Oscillation type of prototype parts
1	165	0	Pistons: contrary displacement.
2	182	0	Pistons: co-direct displacement; case: displacement.
3	294	0	Electromagnet, case, pistons: displacement.
4	407	1	Pistons: contrary inclination.
5	417	1	Pistons: co-direct inclination; case, electromagnet: inclination.
6	489	1	-- * --
7	578	2	Membranes, pistons: sag; case.
8	650	2	Membranes, pistons: sag.
9	669	0	Membranes; sag.
10	670	0	-- * --
11	674	1	-- * --
12	677	1	-- * --
13	691	2	-- * --
14	693	0	Membranes, pistons: sag.
15	694	2	Membranes: sag.
16	698	1	-- * --
17	704	1	-- * --
18	709	0	-- * --
19	737	2	Membranes, pistons: sag.
20	738	2	-- * --
21	765	2	Membranes, pistons: sag, case.
22	772	0	Pistons: contrary sag.
23	778	0	Pistons: co-direct sag; case.

Table 1.1



2.9 Prototype. Calculation (in air).
 Mode shapes.
 a - mode No.1, b - mode No.3, c - mode No.4

and second modes in water is much larger. This is due to the fact that the associated mass of water for the first mode is larger than that for the second mode, the shape of which has the dipole character. Mode No.3 is characterized by the electromagnetic oscillations with respect of the emitter case. Its shape is given in fig.2.9b and its frequency amounts to 294 Hz. The following three modes No.4, No.5 and No.6 have the azimuth index $n = 1$ and are characterized by an inclination of pistons or the electromagnet with respect to the case of the prototype. The shape of mode No.4 is exhibited in fig. 2.9c. Note that the excitation of modes with the numbers 2-6 is due to the asymmetry in the prototype structure. A large group of modes with the numbers 7-21 and the azimuth indices $n = 0, 1$ and 2 is characterized by a deflection of elastic membranes. The eigenfrequencies of these modes in water are practically the same as in air and most of them are also excited due to the structure asymmetry. The natural shapes of modes No.22, No.23 are characterized by a deflection of pistons and the frequencies amount to 772 Hz and 778Hz for antiphase and in-phase deflections of pistons, respectively.

Therefore, the analysis of the frequencies and shapes of the prototype modes has demonstrated that the frequencies of the modes associated with an inclination or deflection of pistons are rather distant from the fundamental mode frequency of the prototype, which determines the "single-mode" character of the prototype structure.

As is mentioned above, the first mode shape is an antiphase displacement of pistons. However, a piston is simultaneously slightly deflected, i.e. the amplitude of the piston centre displacement is larger than the amplitude of the edge displacement of the piston. The difference of these amplitudes is equal to 7.9% of the amplitude of the piston centre displacement.

2.3. Results of prototype tests

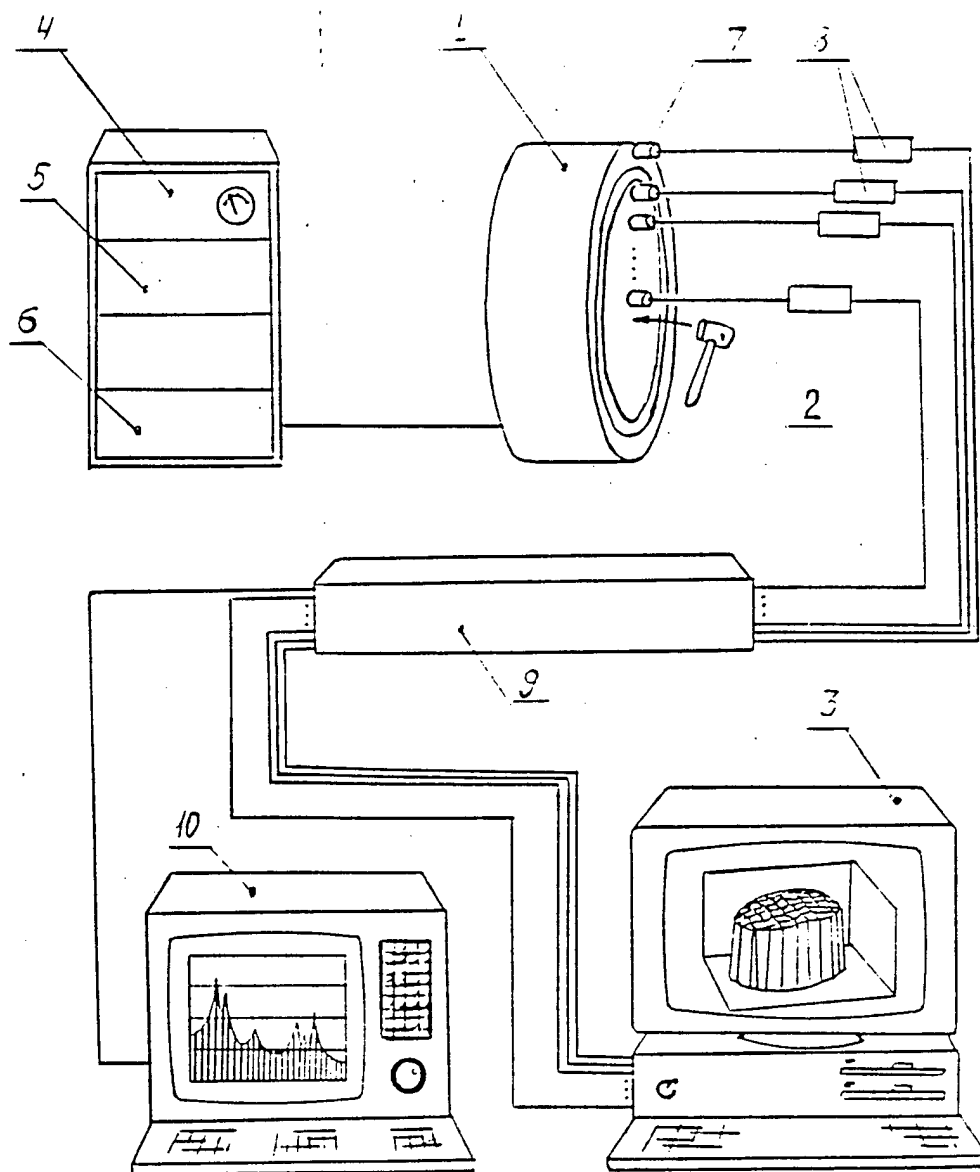
Vibromechanic test of the prototype was performed, the frequency spectrum and the main shapes of forced oscillating were investigated for the broadband and narrowband excitation including that produced by the issued electron excitation system of the

emitter.

A special measuring bench was used to perform vibromechanic tests of the prototype. Its configuration is shown in fig. 2.10. Figure 2.11 deals with the spectrum of the signal obtained from the emitter excited by a short pulse (shock at the piston centre). The maximum spectrum value of 140 Hz corresponds to the operating frequency of the emitter. Other oscillations are concentrated in the frequency band 550-650 Hz. Further analysis has shown that the peak at the frequency 258 Hz is due to the oscillations of the fixed part of the electromagnet which is insufficiently rigidly attached to the case. On the whole, the spectral pattern convincingly proves the single-mode nature of the oscillating system of the emitter. Figure 2.12 displays a similar spectrum obtained under the emitter excitation by the issued inverter, from which it is seen that the excitation coefficient of nonoperating modes is rather small. The single mode character of oscillations in water becomes stronger, since the decrease of the operating mode frequency is much larger than the decrease of other modes. Figure 2.13 depicts the piston displacement shape at the operating mode. It is readily seen that the piston stroke is essentially larger than its deformation value equal to 8% of the piston stroke. Figure 2.14 and 2.15 demonstrate the piston displacement shape in the frequency band 258-620 Hz. Slight asymmetry of the piston displacement is, evidently, the result of the fabrication errors. The resonance frequency of the emitter in air is equal to 140 Hz which is in good agreement with the calculated value. The emitter Q-factor in air is 150. These data can be used to estimate the mechanoacoustic efficiency of the prototype by means of the expression

$$\eta_{ma} = 1 - \frac{f_w Q_w}{f_a Q_a}, \quad (4)$$

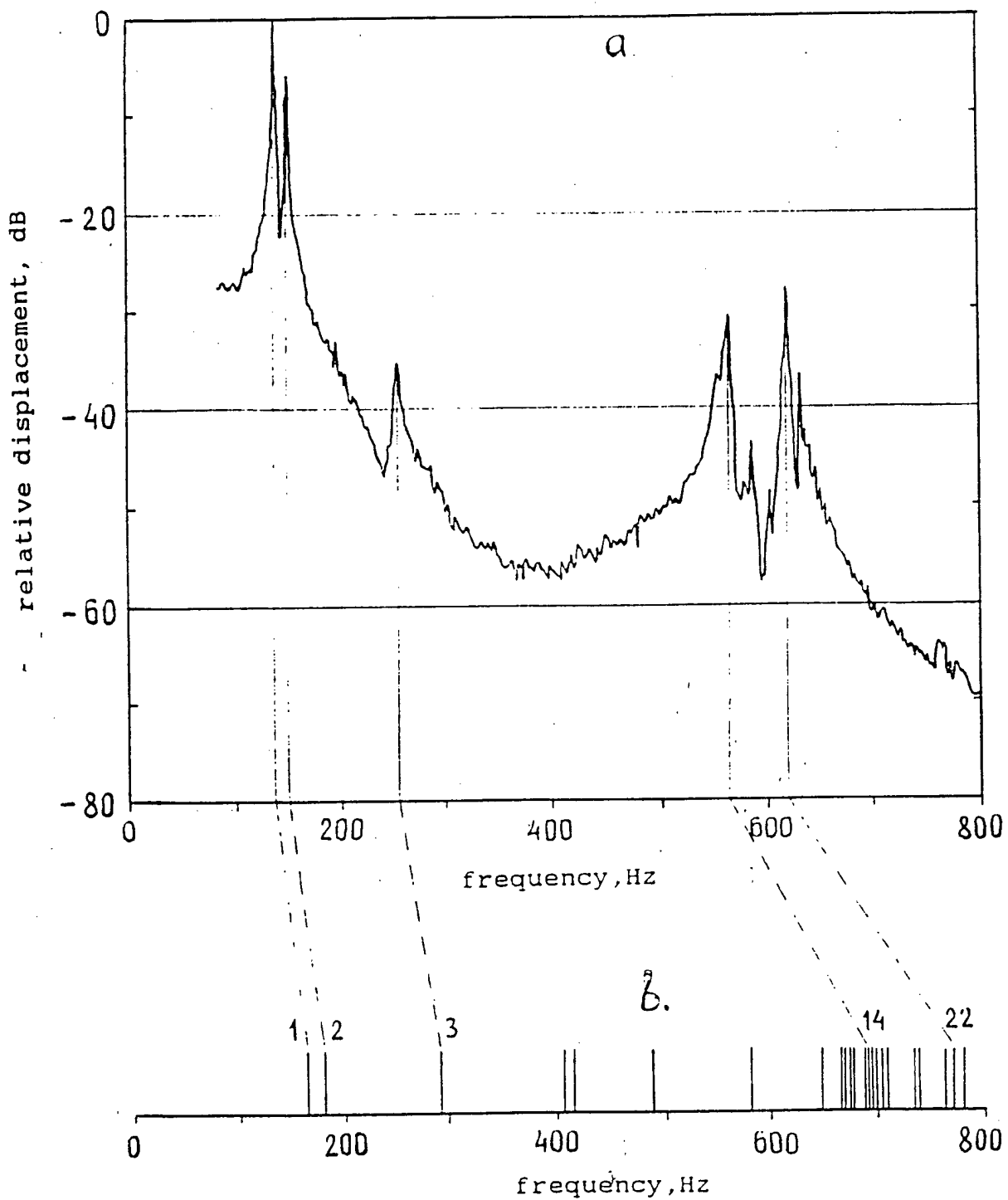
where f_w , Q_w is the frequency and the Q-factor of the mechanical oscillating system in water, f_a , Q_a are the same parameters in air. Substituting the numerical values in Eq.(4) we obtain $\eta_{ma}=96\%$. The obtained efficiency value is typical of the electromagnetic type emitters and is due to the fact that its oscillating system is



- 1 - Source
- 2 - Hammer
- 3 - Computer with interface boards
- 4 - Control unit
- 5 - Power amplifier (invertor)
- 6 - Power Rectifier
- 7 - Vibratory senors
- 8 - Adaptors
- 9 - Multichannel amplifier
- 10 - Spectrum analyzer

2.10

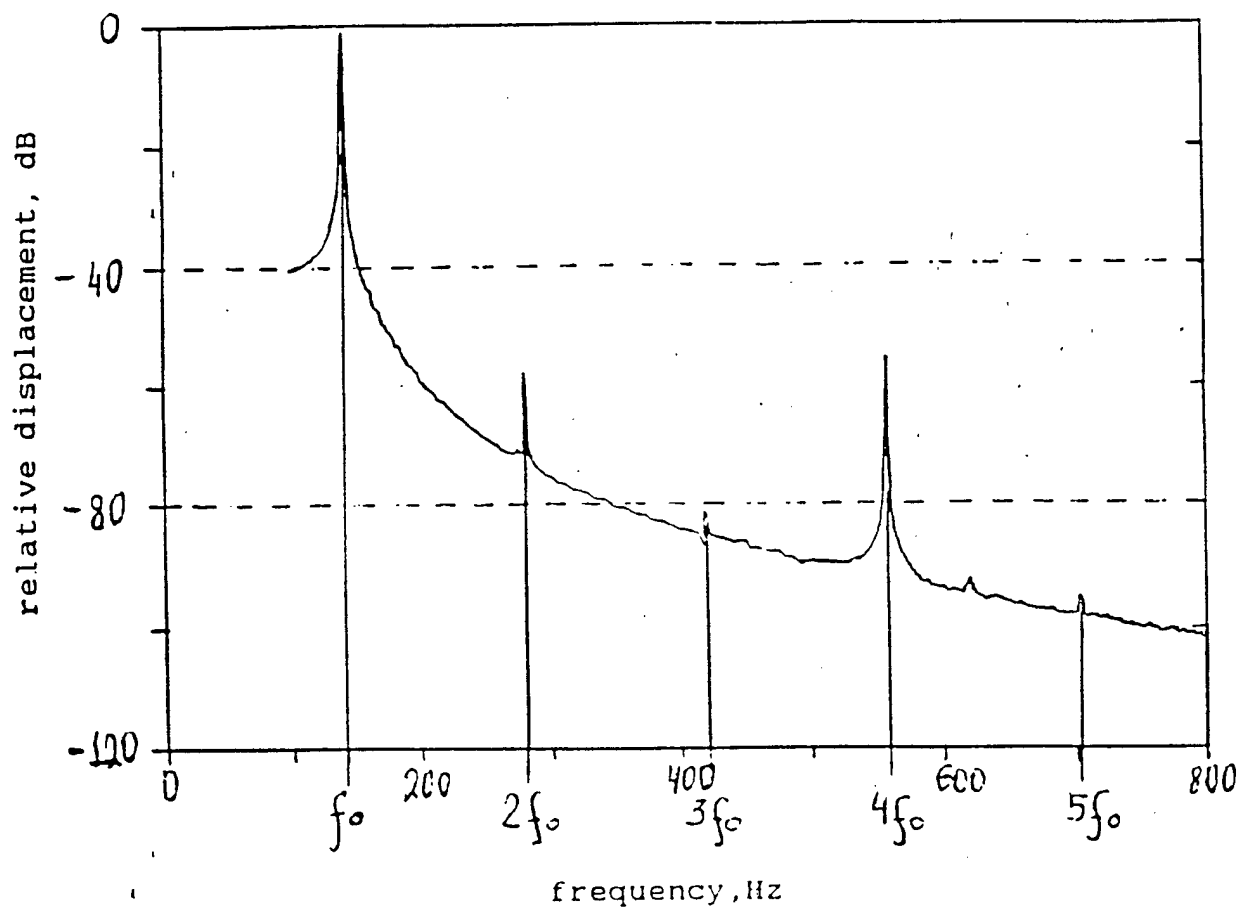
Configuration of the measuring complex for vibro-mechanical tests in air.



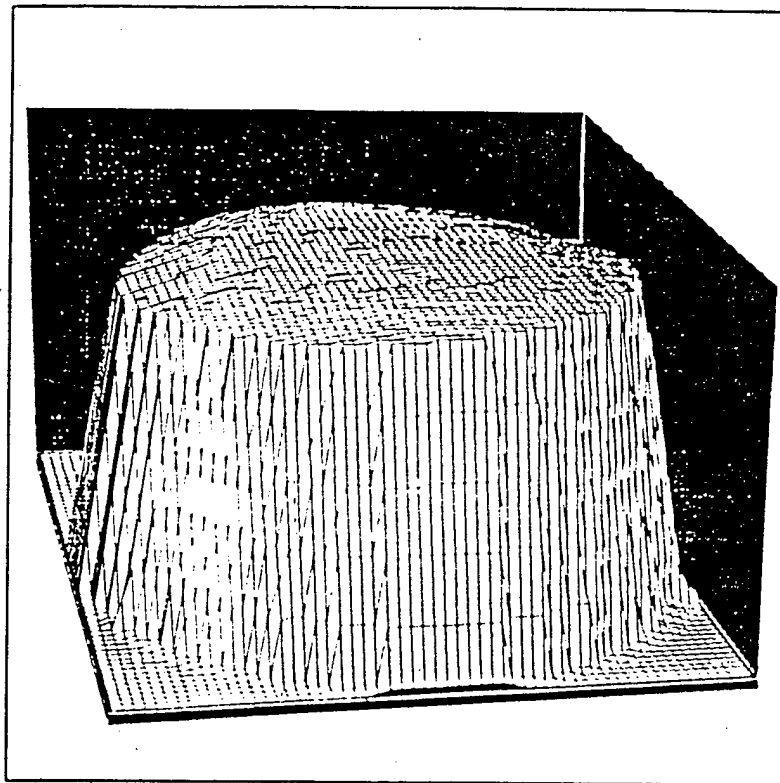
2.11 Prototype.

a - piston centre displacement by shock-excitation (at the same point). Response spectrum averaged over 25 realizations. Experiment (in air).

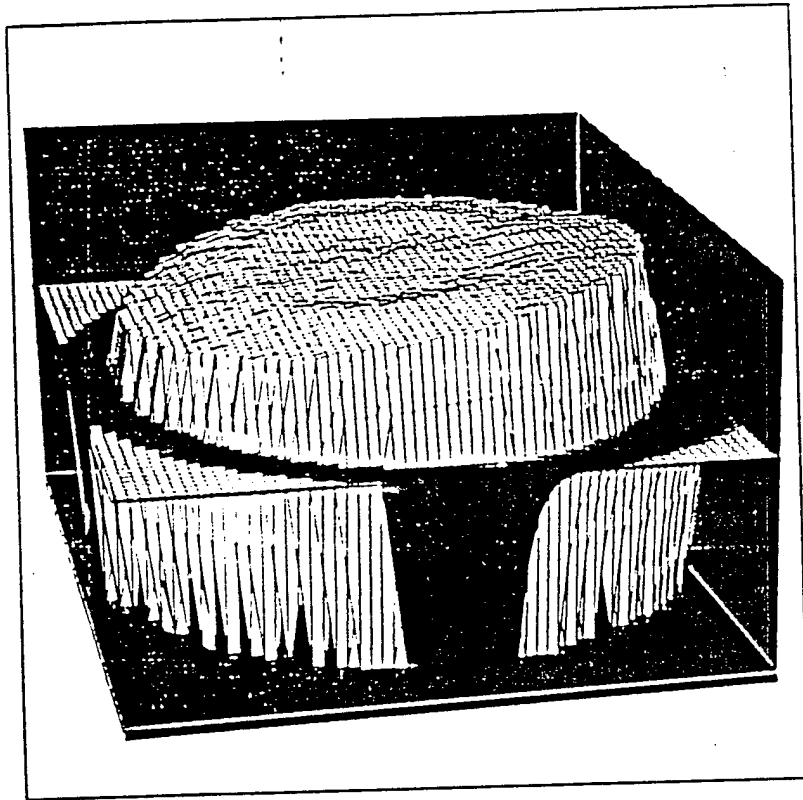
b - mode numbers and frequencies. Calculation.



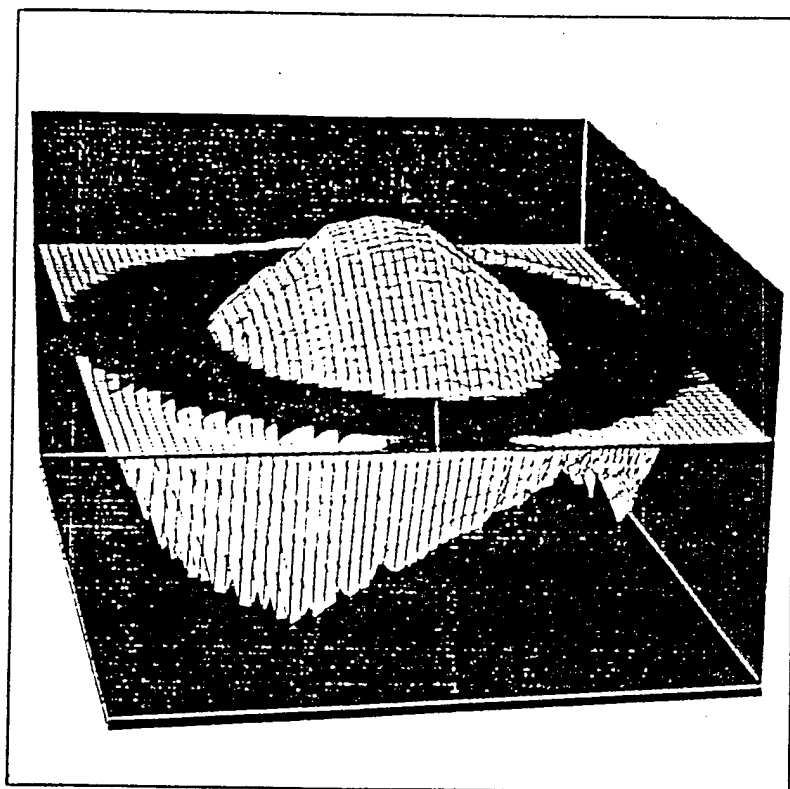
2.12 Prototype. Experiment (in air).
 Forced oscillation spectrum. Displacement of piston centre
 when the source is excited by inverter at an operating mo-
 de. Frequency $f_0 = 142$ Hz.



2.13 Prototype. Experiment (in air).
 Piston displacement shape.
 Oscillation at a frequency $f = 142$ Hz.
 Shape of mode No.1.



2.14 Prototype. Experiment (in air).
Piston displacement shape.
Oscillation at a frequency $f = 258$ Hz.
Shape of mode No.3.

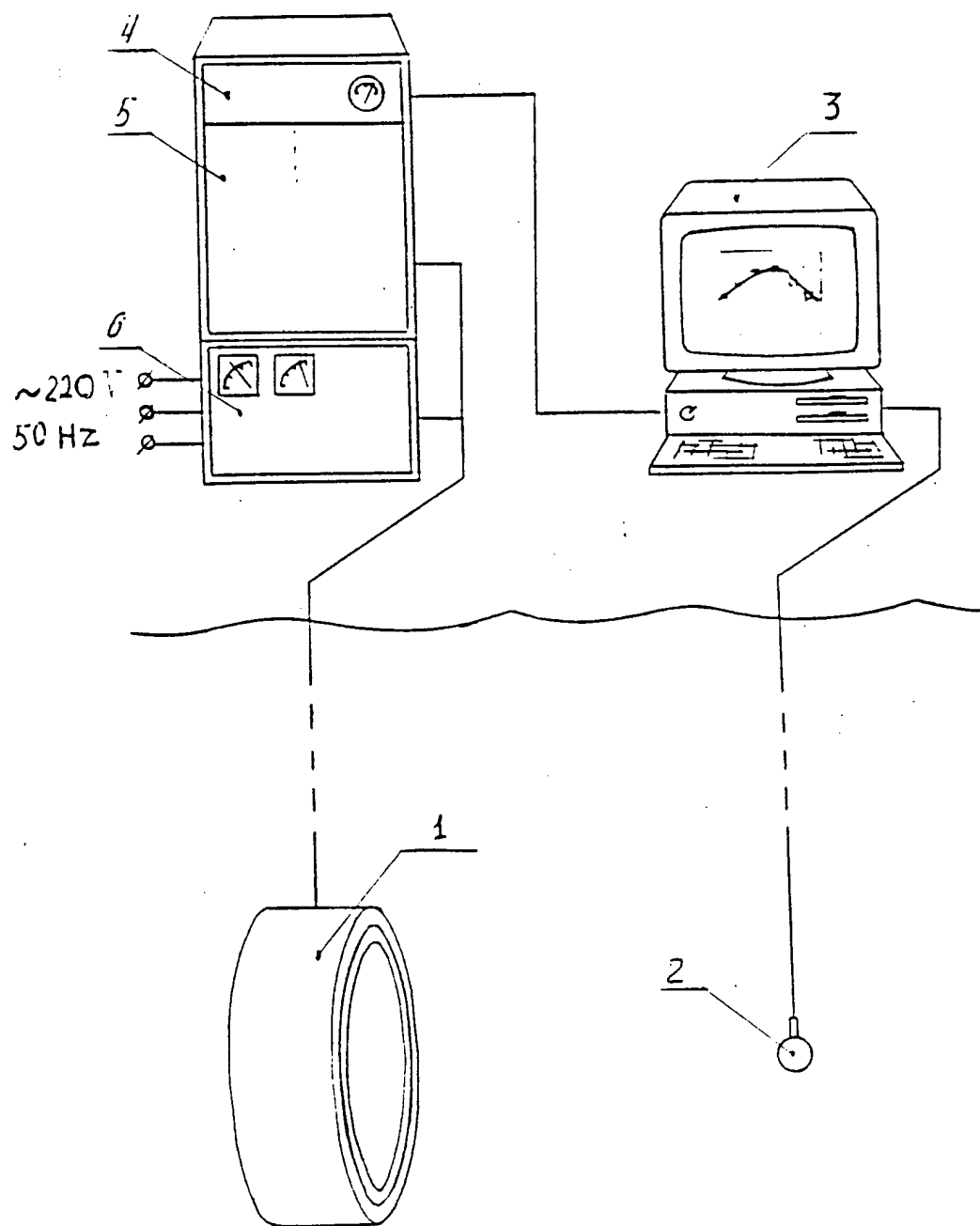


2.15 Prototype. Experiment (in air).
Piston displacement shape.
Oscillation at a frequency $f = 620$ Hz.
Shape of mode No.22.

made of large solid pieces of metal having rather small internal friction. The main places of the energy loss are the attaching points of large structural members. The design and technological techniques are used to provide small mechanical stresses and, thus, small losses.

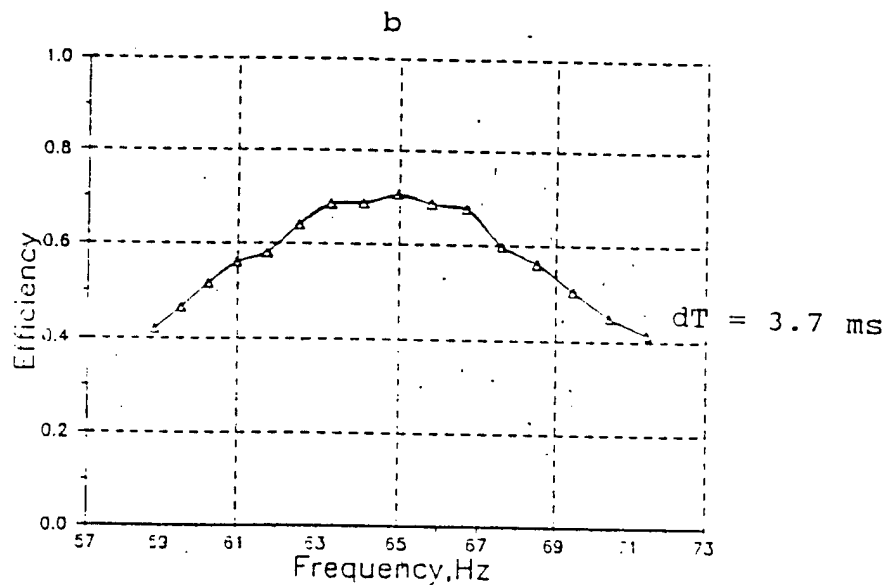
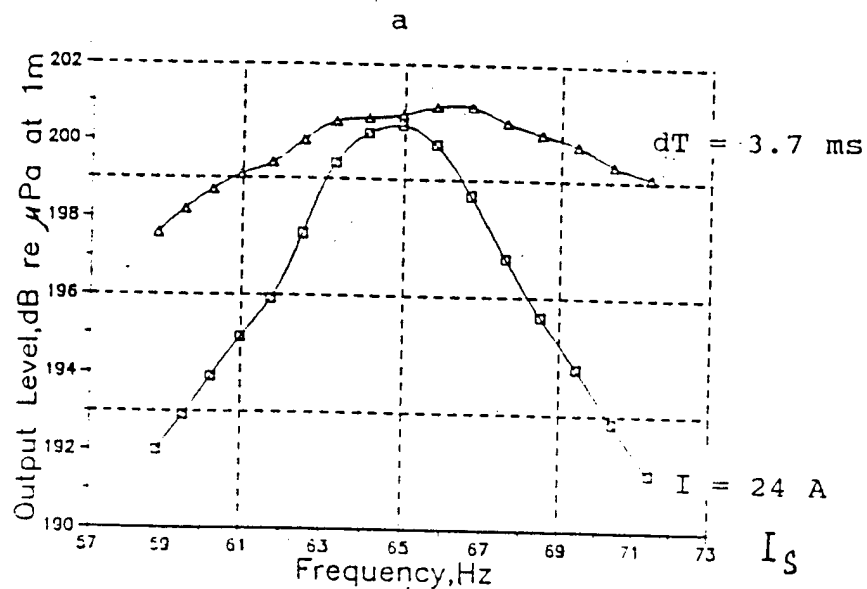
Water tests were performed at the lake. The functional scheme of the water tests is shown in fig. 2.16. The depth of the test was 30m and the emitter submersion depth was 20m. Figure 2.17 displays the frequency characteristic of the emitter at constant current in the magnetic system coil and the frequency characteristic of the emitter when it operates with a thyristor inverter. The resonance frequency in water equals 65 Hz that is by 7% lower than the calculated one, the frequency band is 5 Hz, i.e. 8% of the carrier frequency and coincides with the theoretical one. When operating with the inverter, the frequency band is not less than 14 Hz or 21.5% which is approximately three times wider than the natural frequency band of the emitter. This means that the reserve of the excitation force of the magnetic system is sufficient and the efficiency of the emitter operating with the thyristor inverter is rather high. The efficiency versus the radiation frequency is also plotted. In resonance the efficiency is 70%, at the frequency band edges 40%. The obtained values are close to the calculated ones. Figures 2.18 and 2.19 exhibit the phase-frequency characteristic, the dependences of the radiated power on the excitation current and of the efficiency on the radiation level. The nominal radiation level 201dB is achieved at the current value 21.5 A which is very close to the calculated value.

The comparison of the calculated and experimental parameters presented in Table 1.2 has demonstrated rather good agreement of the results of numerical simulation and tests of the prototype. This enables one to reliably predict the characteristics of the Arctic Source with the resonance frequency 20 Hz using the technique evaluated at the prototype.



- 1 - Source
- 2 - Hydrophone
- 3 - Computer with interface boards
- 4 - Control unit
- 5 - Power amplifier (invertor)
- 6 - Power Rectifier

2.16 Configuration of the measuring complex for acoustic tests in water.



2.17 Prototype. Experiment (in water).

Frequency dependences of output level (a) and efficiency (b) of a piston-type source - inverter system when the source is excited by constant current I_s (\square - \square) or by quasi-constant voltage (\triangle -) at constant input pulse duration T_s .

Parameters:	Calculated	Experimental
Central frequency of emission	70 Hz	65 Hz
Relative operating bandwidth	25 %	21.5 %
Radiation level: nominal maximal		201 dB 204 dB
Efficiency at resonance frequency at level 201 dB	60 %	70 %
Efficiency at band edges		40 %
Source coil current (averaged) at level 201 dB	20 A	20 A
Source coil voltage at level 201 dB	500 V	500 V
Weight		490 kg
Diameter and height		1.1 x 0.5 m
Service life of the source (number of oscillation cycles)	$> 2 \times 10^8$	

Table 1.2 The main parameters of the prototype.

3. Calculation of parameters and numerical simulation of the Arctic Source oscillating system

The method for calculating the emitter parameters and for numerical simulating its oscillating system tested at the prototype, enables one to reliably predict the Arctic Source characteristics with the resonance frequency 20 Hz.

Analysis of the materials employed for the emitter oscillating system and the capabilities of the assumed plant-manufacturer, on the one hand, and of the achievable parameters of the emitter, on the other, has shown that its diameter equal to 1.7m can be taken as a reference one. The emitting area of one piston with the decoupler taken into account is 1.9 sq.m and, thus, the total emitting area of the emitter is 3.8 sq.m, while the equivalent sphere radius amounts to 0.55m. Assuming that the relation between the associated and structure masses for this emitter and for the prototype is approximately equal and that $v_{ma} = 0.7$, we obtain from Eq.(2) the relative frequency bandwidth of the mechanical oscillating system of the emitter, equal to $\delta f = 6.5\%$. It is evident that to obtain the relative band 25%, one should expand the radiation frequency band 3.8 times, which can be provided by the 4-time reserve of strength in the electromagnet. The cross-section of the electromagnet core is found from Eq. (2). For conventional electrical-sheet steel, $B_{max} = 1.7$ T and $S_m = 0.01$ m², for electrical-sheet steel with the increased saturation induction $B_{max} = 2.2$ T we have $S_m = 0.006$ sq.m. The design analysis has shown that a larger cross-section of the electromagnet core may be used without impairment of other parameters of the emitter. In this case S_m is chosen to be 0.02 sq.m and the electromagnet core material is transformer electrical-sheet steel with $B_{max} = 1.7$ T, which guarantees the obtainment of the necessary frequency band.

The radiation power of the monopole is related to the oscillation amplitude of the emitting area by the expression

$$N = \frac{\rho \omega^4 S_1^2 \delta^2}{8 \pi C}, \quad (5)$$

where δ is the oscillation amplitude of the emitting area. For the power 1kW, $\delta = 3.2$ mm. To provide the required piston stroke, the gap between the moving and fixed parts of the magnetic system calculated following that the electromechanical efficiency of the emitter at the frequency band edges should not be less than 80%, are presented below. The number of loops in the coil is 320, the number of windings is 2, and the wire cross-section is 8.25 sq.mm. The nominal power in the resonance is achieved at the average current in the winding 10 A and at the voltage 750 V. The current at the frequency band edge equals 16 A, while the voltage is 1500 V. The emitter with a magnetic system on the scale 1:5 is shown in fig. 3.1.

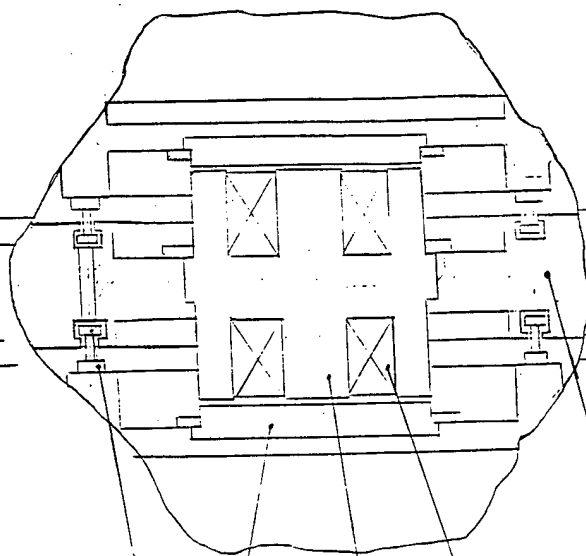
The piston with the decoupler and the flange is presented in fig. 3.2. It is made of the D 16 T duralumin alloy plate 120 mm thick. As distinct from the prototype, the elastic decoupler is made as the bellows half-wave, which enabled us, on the one hand, to provide the necessary piston stroke at allowable mechanical loads in the decoupler and, on the other hand, to increase the emitting area.

Numerical simulation of the emitter was performed by analogy with that of the prototype to determine the spectrum of eigenfrequencies of the emitter in air and to estimate maximum stresses in the structure oscillating at the fundamental mode frequency and for excess internal status pressure.

The pilot finite-element model of the emitter had 1130 units and 647 axially symmetrical elements.

Figure 3.3 displays the arrangement of the first 29 modes with the azimuth indices $n = 0, 1$ and 2 on the frequency axis. The number, frequency, azimuth index and the structure oscillation type are given for each mode in Table 3.1. Modes No.1 and No.2 (by analogy with modes No.1 and No.2 of the prototype) are the operating monopole and dipole modes of the emitter, respectively. Their frequencies are 52 Hz and 67 Hz. The difference between the frequencies of these modes in water is large, since the associated mass of monopole oscillations is larger than that of dipole ones.

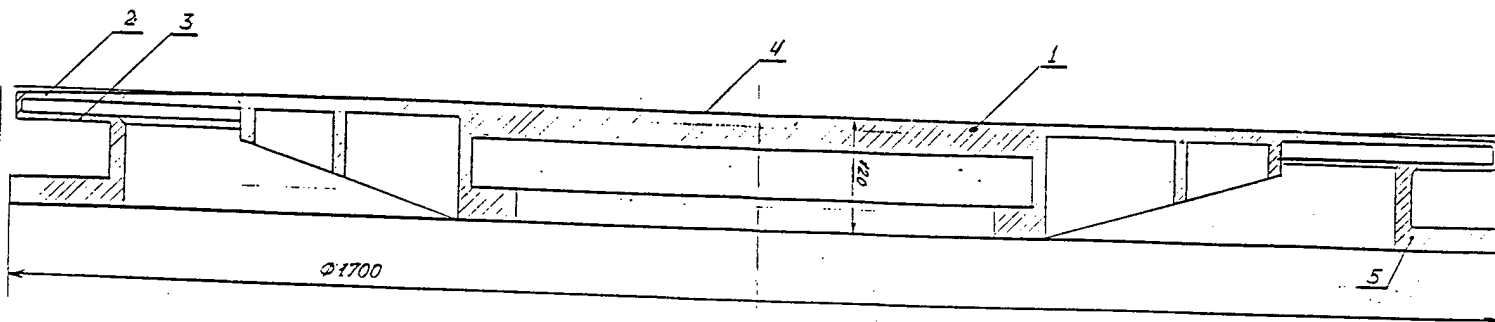
61700



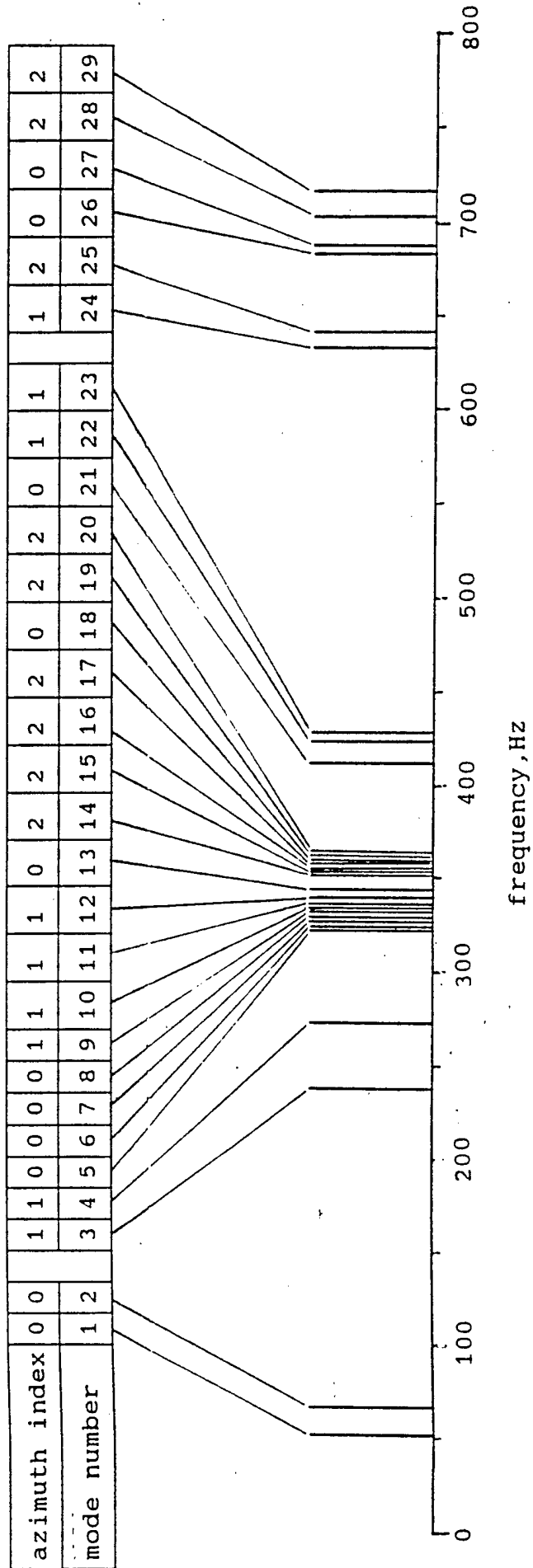
- | | |
|--------------------------------------|-------------|
| 1 - Electromagnet Core (fixed part) | 4 - Piston |
| 2 - Electromagnet Core (moving part) | 5 - Case |
| 3 - Field Coil | 6 - Stopper |

34

3.1 20 Hz source.
Scale 1:5



- 1 - Piston part
- 2 - Hermetic decoupler (part 1)
- 3 - Hermetic decoupler (part 2)
- 4 - Radiating surface
- 5 - Flange



3.3 20 Hz source. Calculation (in air).
Mode frequencies.

Mode number	Frequency Hz	Azimuth index	Oscillation type of source parts
1	52	0	Pistons: contrary displacement.
2	67	0	Pistons: co-direct displacement; case: displacement.
3	238	1	Pistons: contrary inclination.
4	273	1	Pistons: co-direct inclination; case: inclination.
5	327	0	Hermetic decouplers.
6	328	0	-- * --
7	330	0	Membranes; sag.
8	330	0	-- * --
9	332	1	-- * --
10	334	1	-- * --
11	336	1	-- * --
12	339	1	-- * --
13	343	0	Electromagnet, case, pistons: displacement; membranes: sag.
14	349	2	Membranes; sag.
15	353	2	-- * --
16	354	2	Hermetic decouplers.
17	355	2	-- * --
18	357	0	Membranes; sag.
19	358	2	-- * --
20	359	2	-- * --
21	413	0	Electromagnet, case, pistons: displacement; membranes: sag.
22	424	1	Hermetic decouplers; pistons: inclination.
23	427	1	-- * --
24	638	1	Electromagnet, case, pistons: inclination.
25	643	2	Case.
26	686	0	Pistons: contrary sag.
27	687	0	Pistons: co-direct sag.
28	703	2	Pistons: sag.
29	717	2	-- * --

Table 3.1

The mode arrangement on the frequency axis of the prototype and of the emitter and their spectra are similar. This is due to the fact that the prototype and the emitter are designed similarly and include the same basic elements: piston, elastic membrane and a case with an electromagnet. These elements determine the modes of the prototype and of the emitter in the considered frequency range.

In both spectra there are:

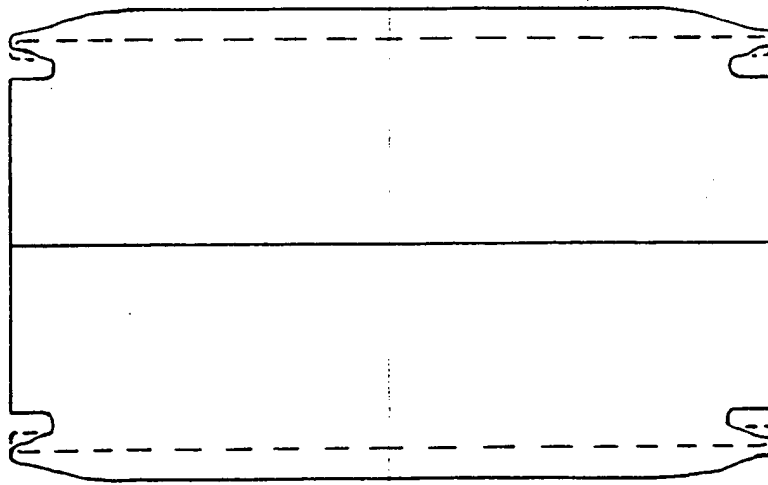
- two modes of antiphase and in-phase displacement of pistons (mode No.1 and No.2 of the prototype and of the emitter);
- two modes of piston inclination (modes No.4, No.5 of the prototype and modes No.3, No.4 of the emitter);
- twelve modes (four modes with each azimuth index $n = 0, 1$ and 2) of elastic membrane deflection (modes No.9 ... No.20 of the prototype and modes No.7 ... No.12, No.14, No.15, No.18... No.21 of the emitter);
- one mode of the electromagnet inclination (mode No.6 of the prototype and mode No.24 of the emitter);
- four modes (two with each azimuth index $n = 0$ and 2) of piston inclination (modes No.8, No.21 ... No.23 of the prototype and modes No.26 ... No.29 of the emitter);
- one mode of the case deflection (mode No.7 of the prototype and mode No.25 of the emitter).

Figure 3.4a exhibits the shape of the fundamental mode No.1 of the emitter. Figure 3.4b and 3.4c deals with the shapes of the modes associated with the piston inclination (mode No.3) and with the electromagnet displacement (mode No.13), respectively.

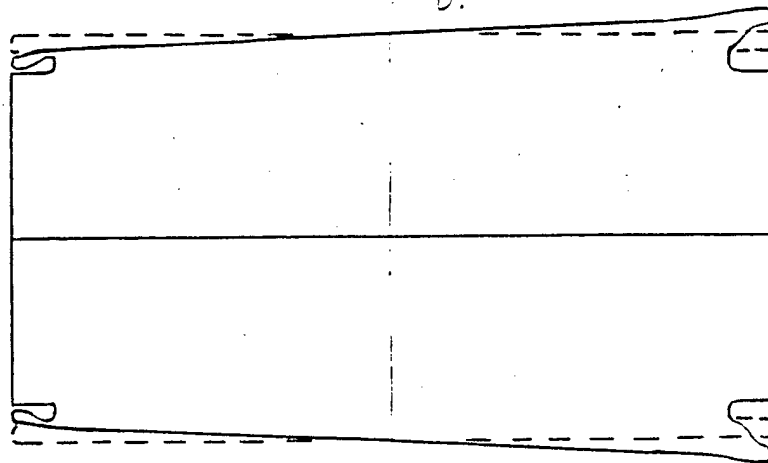
The differences in the design of the prototype and of the emitter result in differences of mode spectra. The transition part of the emitter piston is of different shape, which leads to the occurrence of new modes in its spectrum. These modes are six (two modes with each azimuth index $n = 0, 1$ and 2). They are the emitter modes with the numbers 5, 6, 16, 17, 22, 23.

Let us compare now the relative arrangement of analogous modes in the spectra of the prototype and of the emitter. This arrangement is due to the parameters of basic design elements, their effective elasticity and mass. Thus, e.g., the enhanced rigidity of the electromagnet attachment to the emitter case has increased the frequencies of the modes produced by displacement and inclination of the electromagnet (modes No.13 and No.24 of the

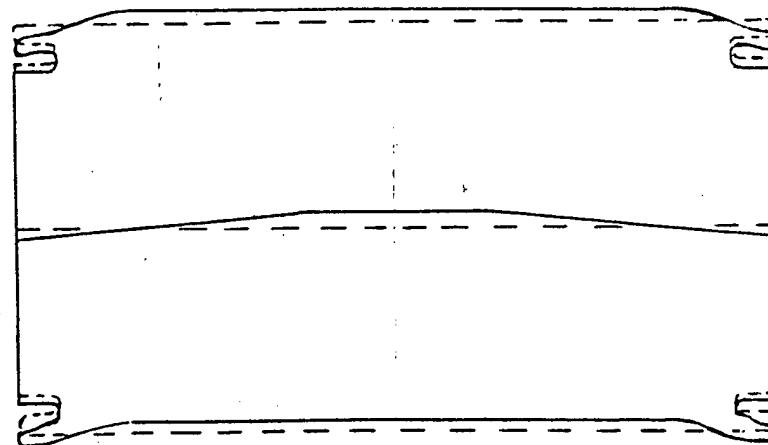
a.



b.



c.



3.4 20 Hz source. Calculation (in air).
Mode shapes.
a - mode No.1, b - mode No.3, c - mode No.13

emitter). The corresponding modes of the prototype (modes No.3 and No.6) are relatively closer in frequency to the fundamental mode. The enlarged distance between the elastic membrane bases has relatively increased the mode frequencies, caused by piston inclination (modes No.3 and No.4 of the emitter and modes No.4 and No.5 of the prototype).

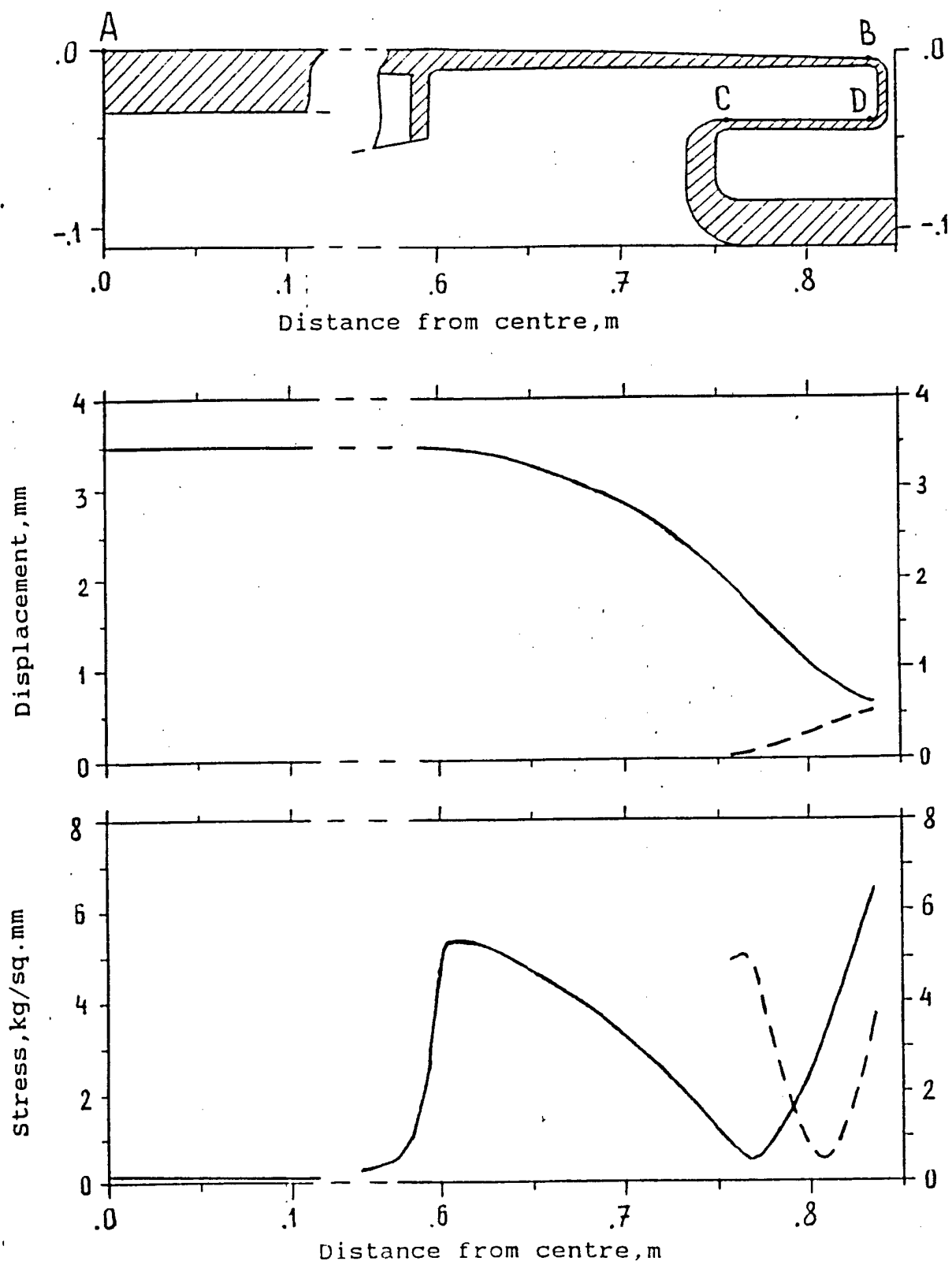
Therefore, the analysis of the emitter mode has demonstrated that the frequency of the fundamental mode of the emitter is essentially distant from the frequencies of other modes and, thus, the emitter structure is of the "single-mode" character.

Figures 3.5 and 3.6 show the distributions of the displacement amplitude and of the stress intensity along the piston radius and the membrane spring oscillating at the first mode frequency 52 Hz. The displacement amplitude of the piston edge differs from that of the piston centre by the value of 5% (the relative piston deflection). The stress intensity G at this point is determined by the relation $G = G_1 - G_3$, where G_1 and G_3 are the maximum and minimum principal stresses at this point. The maximum stress intensity is observed close to the point B of the transition part of the piston and amounts to $G = 7.1 \text{ kg /sq.mm}$ for the piston displacement amplitude $d = 3.5 \text{ mm}$. In this case the maximum stress intensity in the membrane spring does not exceed 5.5 kg/sq.mm . Therefore, the mechanical stress in the basic structure elements are rather small, which permits to provide the necessary service life of the emitter (fig. 2.7).

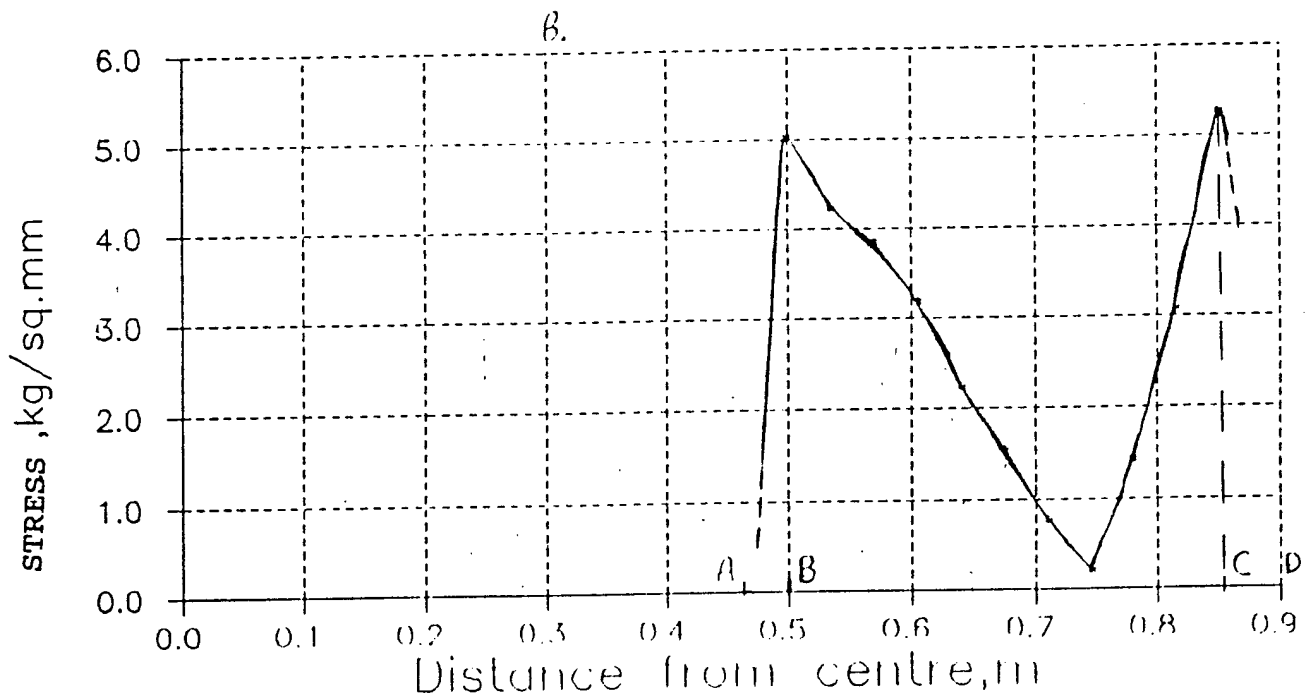
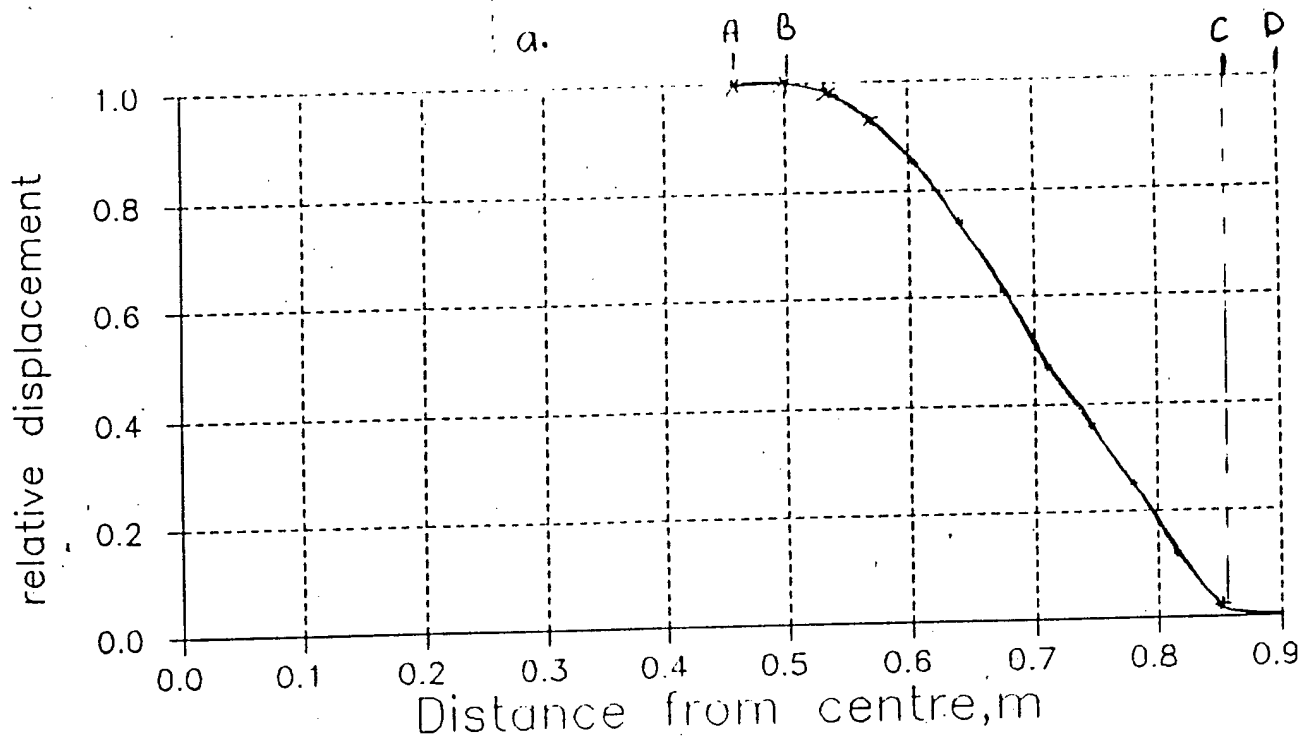
At low frequencies the air elasticity in the internal cavity of the emitter becomes close to the spring elasticity. The air elasticity coefficient is yielded by

$$k_a = \frac{\kappa P S_1^2}{V_1}, \quad (6)$$

where κ is the polytrope index, P is the air pressure inside the emitter, and V_1 is the air volume in the emitter. Since the air pressure in the emitter is to be equal to the hydrostatic pressure of water at the emitter submersion depth, the air elasticity increases proportionally with the depth and, thus, if k_a is comparable or larger than the emitter elasticity, the resonance frequency increases with the depth. The emitter should provide radiation in the given frequency band at any point of the



- 3.5 20 Hz source. Calculation (in air).
 Radiating element (c).
 Displacement (a) and stress (b) profiles.
 Oscillations at an operating mode.
 Frequency $f = 52$ HZ.
 Solid line - in section AB (piston and decoupler),
 dashed line - in section CD (decoupler).



3.6 20 Hz source. Membrane (spring). Calculation.
 Relative displacement (a) and stress (b) profiles
 (Displacement amplitude 3.5 mm).
 Section AB - inside flange, section BC - spring
 element.

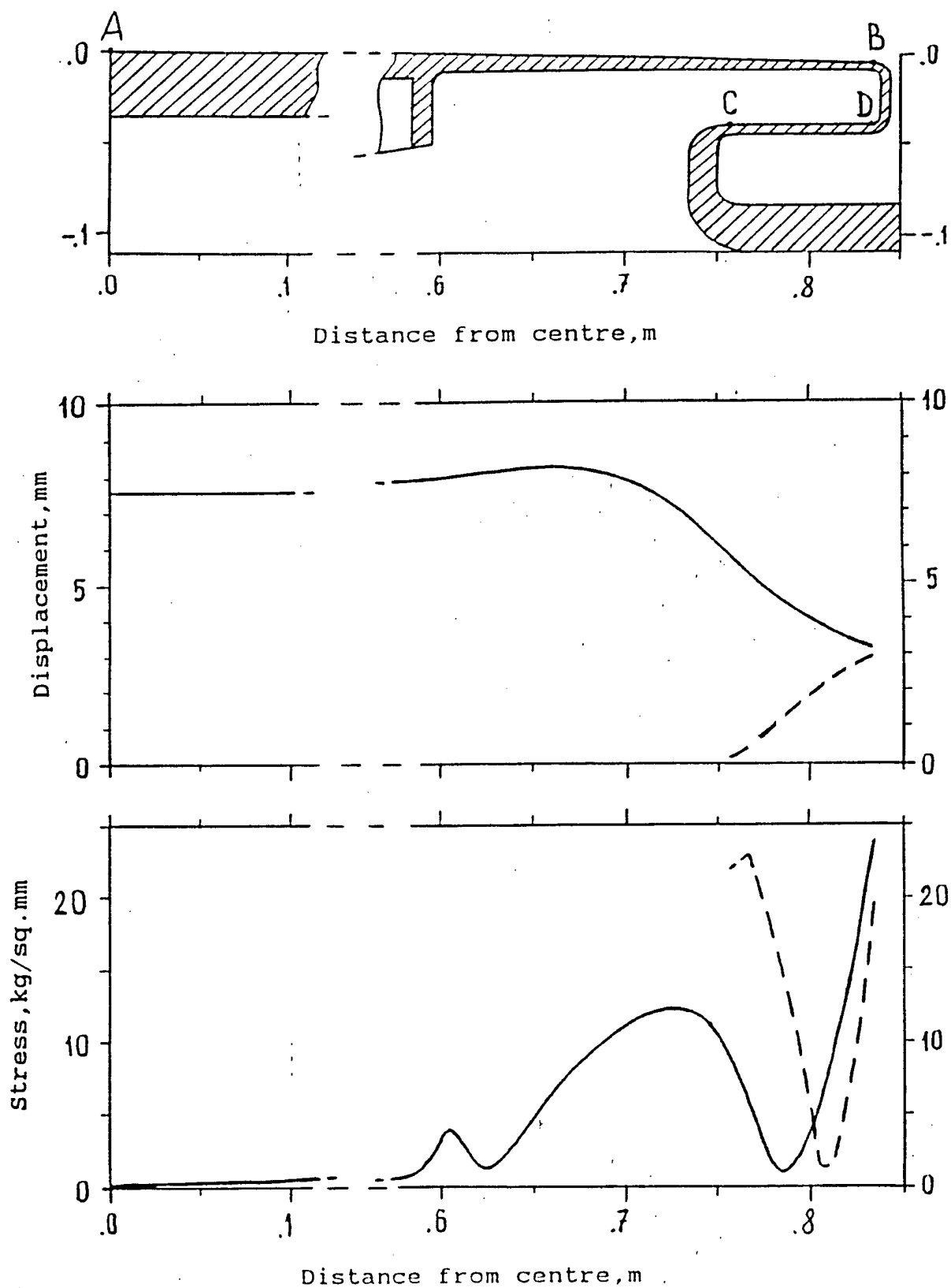
operating depth range down to the maximum depth used. The total oscillating mass of the emitter with the associated mass of water equals 2700 kg and, hence, its elasticity coefficient is 4.3×10^7 N/m at the resonance frequency 20 Hz.

Following that the resonance frequency change of the emitter when it is submerged at the depth from 100 to 150 m should not exceed 50% of its frequency band and using Eq.(6), we obtain that the air cavity volume of the emitter is $V_1 = 1.1 \text{ m}^3$. It is designed that $V_1 = 1.5 \text{ m}^3$.

Let us consider now the emitter structure stress for the excess internal static pressure. The emitter design provides for the maximum piston displacement of $h = 7.5$ mm. This value is achieved at the excess internal pressure $p = 1.17$ kg /sq.cm. The maximum stress intensity is $G = 20.2$ kg /sq.mm. Figure 3.7 depicts the distributions of the displacement and of the stress intensity along the piston radius at the excess internal pressure of $p = 3$ kg /sq.mm = 3 techn.atm. In this case the piston reaches the stoppers (fig.3.1), the maximum displacement in the transition part of the piston amounts to $d = 8.15$ mm, while the maximum stress intensity is observed close to the point B and equals $G = 28.6$ kg /sq.mm. Note that the excess internal pressure of up to 3 techn.atm. previously created in the emitter, enables one to submerge it in water to a depth of 30 m without employing hydrostatic pressure compensators.

The main characteristics of the Arctic Source are given in Table 3.2.

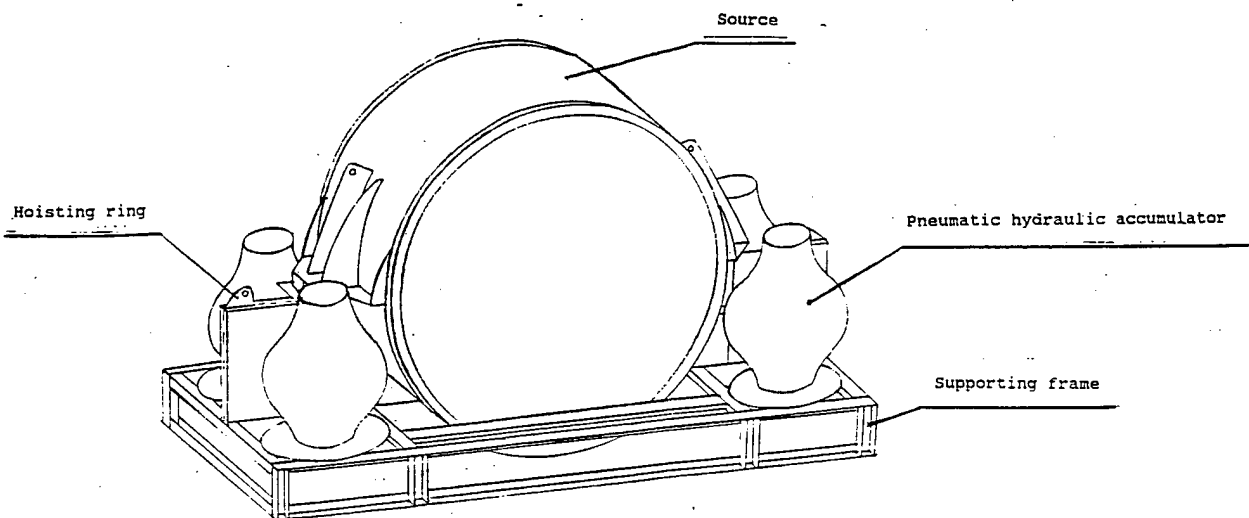
Figures 3.8 and 3.9 show the submerged emitting module and the underwater part of the emitting complex in the operative position. The Arctic Source manufacture schedule is given in Table 3.3.



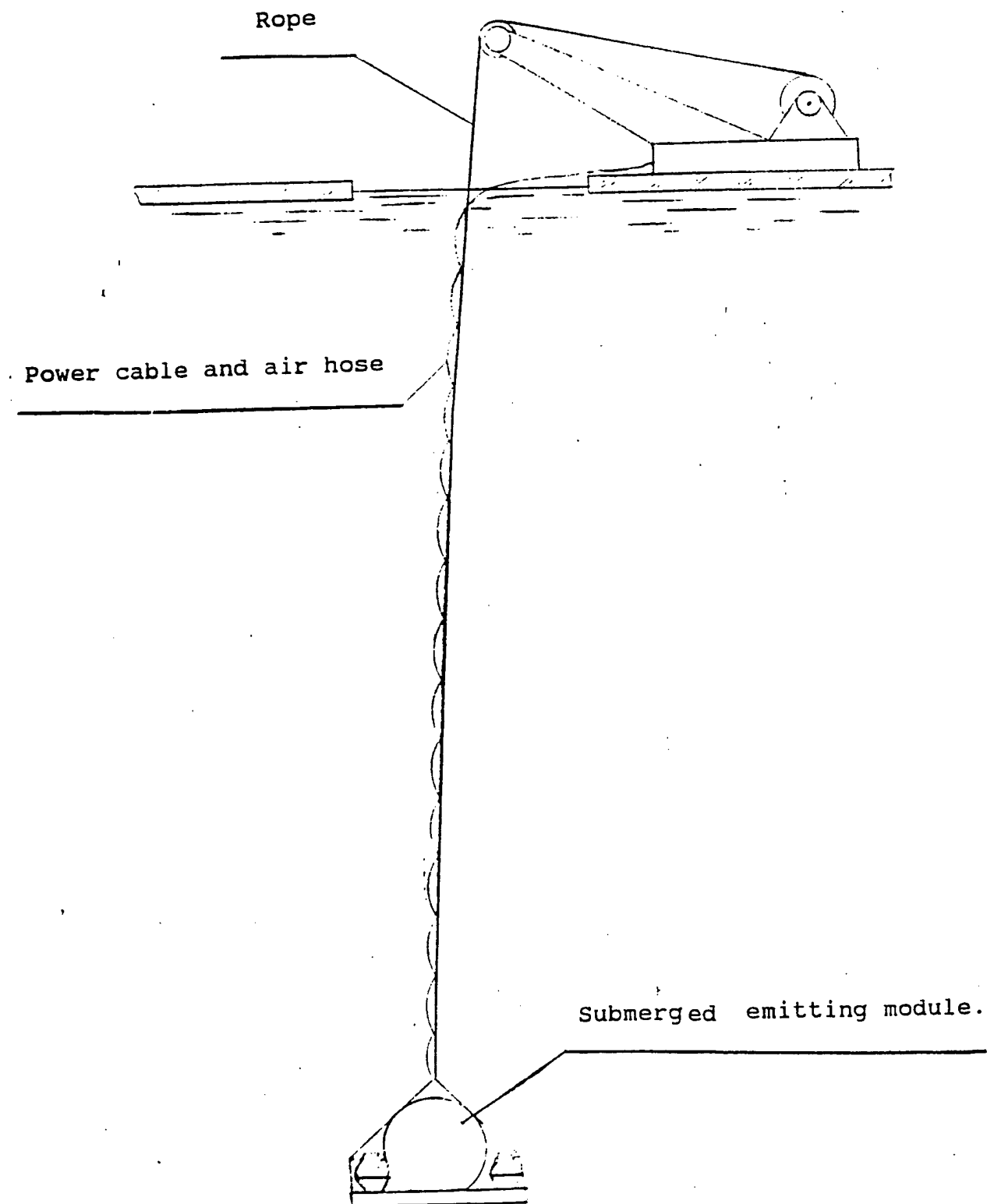
3.7 20 Hz source. Calculation (in air).
 Radiating element (c).
 Displacement (a) and stress (b) profiles.
 Statis. Internal surplus pressure $P = 3$ atm.
 Solid line - in section AB (piston and decoupler),
 dashed line - in section CD (decoupler).

Parameters:	Calculated
Central frequency of emission	20 Hz
Relative operating bandwidth	25 %
Radiation level: nominal maximal	201 dB 205 dB
Efficiency at resonance frequency	60-70 %
Source coil current (averaged) at level 201 dB	10 A
Source coil voltage at level 201 dB	750 V
Weight	1500 kg
Diameter and height	1.7 x 1 m
Service life of the source (number of oscillation cycles)	> 2 x 10 ⁸

Table 3.2 The 20 Hz source main parameters.Calculation.



3.8 Submerged emitting module.



3.9 Underwater part of the emitting complex in operation position.

No.	Works contents	1993		1994				Executors
		XI	XII	I	II	III	IV	
1	Source production documents development	—	—					ASTC "GRAN"
2	Tooling design and manufacture	—	—					"ZFS" plant
3	Source metal and materials manufacture		—	—				"Stupino" plant
4	Source manufacture			—	—	—		"ZFS" plant
5	Pressure compensation system production documents development		—	—				CDO "Lazurit"
6	Underwater module production documents development		—	—				CDO "Lazurit"
7	Pressure compensation system manufacture			—	—	—		"Krasnoe Sormovo" plant
8	Underwater module manufacture			—	—	—		"Krasnoe Sormovo" plant
9	Source and underwater module assembly and joint tests					—		ASTC "GRAN", "Krasnoe Sormovo" plant
		XI	XII	I	II	III	IV	
		1993		1994				

Table 3.3 The Arctic Source manufacture schedule.

4. Conclusion

Let us formulate the main results obtained.

1. Using the conception of developing effective monopole low frequency emitter based on single-mode oscillating systems, elaborated earlier, an emitter with the resonance frequency 20 Hz has been designed for use during the Arctic Feasibility Acoustic Propagation Pilot Test.
2. The basic parameters of the Arctic Source have been calculated and its oscillating system has been simulated numerically, which proved the feasibility of the designed technical characteristics.
3. The methods for calculating the basic parameters and for numerical simulating the oscillating system were tested at the emitter prototype with the resonance frequency 65 Hz. The results of the simulation and of the vibromechanical and acoustical tests of the prototype are in rather good agreement, which enables one to reliably predict the Arctic Source characteristics.
4. The plant is determined where the emitter will be fabricated, the production plan is coordinated, the emitter structure is analysed, the technological background of the production is provided, the problems of the material and element supply are discussed, and the schedule of the Arctic Source fabrication is developed.

REFERENCES.

[1] Evaluation of Electromagnetic Source for Ocean Climate Acoustic Thermometry at Lake Seneca. Woods Hole Oceanographic Inst. Tech. Rept., WHOI-93-09.

[2] M.Slavinsky, B.Bogolubov and J.Spiesberger.
Low-Frequency, High Efficiency Sources for Acoustic Monitoring of Climatic Temperature Changes in Ocean Basins.
J.A.S.A, Vol.92, No 4, Pt.2, October 1992.

[3] Requirements Analysis for the Design of an Installation of an Acoustic Emission System in the Far East of Russia as a Part of the ATOC Network in the North Pacific Ocean. ASTC Tech. Rept., 1993.